J. Appl. Comput. Mech., 5(5) (2019) 875-899
DOI: 10.22055/JACM.2019.27297.1397

ISSN: 2383-4536
jacm.scu.ac.ir

Archive of SID

M&MoCS

Shahid Chamran University of Ahvaz

Journal of Applied and Computational Mechanics



Research Paper

On Bending Response of Doubly Curved Laminated Composite Shells Using Hybrid Refined Models

J.C. Monge[1], J.L. Mantari[1], J. Yarasca[1], R.A. Arciniega[2]

[1] Faculty of Mechanical Engineering, National University of Engineering, Av. Túpac Amaru 210, Rimac, Lima, Peru
[2] Department of Civil Engineering, Universidad Peruana de Ciencias Aplicadas (UPC), Surco, Lima, Peru

Received October 18 2018; Revised March 09 2019; Accepted for publication April 16 2019.
Corresponding author: J.L. Mantari, jmantari@utec.edu.pe
© 2019 Published by Shahid Chamran University of Ahvaz
& International Research Center for Mathematics & Mechanics of Complex Systems (M&MoCS)

Abstract. This paper presents a static analysis of laminated composite doubly-curved shells using refined kinematic models with polynomial and non-polynomial functions recently introduced in the literature. To be specific, Maclaurin, trigonometric, exponential and zig-zag functions are employed. The employed refined models are based on the equivalent single layer theories. A simply supported shell is subjected to different mechanical loads, specifically: bi-sinusoidal, uniform, patch, hydrostatic pressure and point load. The governing equations are derived from the Principle of Virtual displacement and solved via Navier-Type closed form solutions. The results are compared with results from Layer-wise solutions and different higher order shear deformation theories available. It is shown that refined models with non-polynomial terms are able to accurately predict the through-the-thickness displacement and stress distributions maintaining less computational effort compared to a Layer-wise models.

Keywords: Shell, Laminated composite, Carrera Unified Formulation (CUF), Doubly-curvature.

1. Introduction

Multilayered shell structures are employed in many engineering fields such as aerospace, naval and automotive due to their superior characteristics. Shells are curved structures which have excellent load-carrying capacity in comparison to plates. Moreover, composite materials provide several attractive properties as high strength, high stiffness-to-weight ratio, corrosion resistance, acoustic insulation and a remarkable fatigue life [1]. The use of composite structures lead the development of different computer codes to study the mechanical behavior for different laminations and geometries [2]. Consequently, reliable and efficient computational models for multilayered structures are still an interesting and important research topic.

Linear elastic thin shell theories have been formulated for over 70 years. Main contributions based on the classical shell theory (CST) were presented by: Timoshenko and Woinowsky-Krieger [3], Flügge [4], Leissa [5], Gould [6] and Soedel [7]. Those contributions were based on the investigations developed by Love [8]. The CST shows inaccuracies for anisotropic and thick shells since it neglects the transverse shear and normal stresses. The First order shear deformation theory (FSDT) was proposed by Hildebrand et al. [9] in order to include the effect of transverse shear stress. As is well known, the FSDT depends on a shear correction factor, which is difficult to estimate for composite shells. Consequently, the Higher Order Shear Deformation theories (HSDTs) [10-15] were reported on the literature. HSDTs include additional terms on the kinematic model in order to accurately predict the laminated composites displacements and stress distributions.

A generalization of HSDTs is the so-called Unified Formulations (UFs) [16-19]. UFs allows writing arbitrarily and a large variety of 2D models, these are obtain by varying the order of expansion of the selected thickness functions. Investigations on HSDTs that include polynomial [20-23] and non-polynomials [24-31] functions have shown the full capacity of HSDT. However, for the search of refined shear deformation theoretical model, the fact that in some HSDTs the number and type of

Published online: May 25 2019

www.SID.ir

Archive of SID

shear strain shape functions is defined *a priori* and consequently the kinematic model is studied independently is a clear disadvantage compared with UFs. An excellent review on plate and shell theories for laminated and sandwich structures comparing HSDTs and UFs were presented by Caliri et al. [21].

The present formulation is developed based on Carrera's Unified Formulation (CUF) with the inclusion of non-polynomial expansion function to study shells for the first time. According to CUF, the displacement field of the shell can be defined as an arbitrary expansion of the thickness coordinates. The governing equations are the so-called fundamental nuclei whose form does not depend on either the expansion order nor on the choices made for the shear strain shape functions. A unified formulation based on CUF is used for solving different problems such as: mechanical [27-32] and thermo-mechanical problems [33, 34] and piezo-electric [35, 36]. The highly coupled differential equations are solved via Navier type solutions and several static problem of shells subjected to localized, point and distributed loads are analyzed.

Shell multilayered models can be implemented in two different approaches: Equivalent Single Layer (ESL) and Layer-wise (LW) [16-18]. An ESL model considers multilayered structures as a single equivalent layer. A LW model maintains each lamina separately; therefore, accurate displacements and stress distributions are obtained in comparison to ESL models. However, the high computational cost of LW models makes it difficult for engineering applications. Thus, robust ESL models with adequate precision are preferred.

A vast number of investigations have been presented regarding shell's behavior. Giunta et al. [37] presented a unified formulation for the modeling of doubly-curved laminated shells. Tornabene et al. [38] presented a stress recovery method with CUF and the differential geometry tool to obtain quasi-3D results for doubly-curved anisotropic shells and panels. Dozio [39] used a space-state approach in conjunction to Levy's Method for solving free vibration problem of spherical and cylindrical panels by applying a hierarchical formulation. Viola et al. [40, 41] presented a new HSDT for free vibration and static analysis of shells. Differential geometry was employed to define the arbitrary shape of the middle surface of shells with different curvatures. The authors investigated numerical solution of differential equations based on generalized differential quadrature technique. Tornabene et al. [42] applied CUF for the free vibration of doubly-curved laminated shells and panels, the highly coupled differential equation were solved numerically applying radial basis functions. Thinh et al. [43] investigated the free and forced vibration of thick laminated composites cylindrical shells by the continuous element method constructed from the dynamic stiffness matrix. Cinefra and Valvano [44] combined CUF and mixed interpolation of tensorial component for solving different problems of anisotropic doubly-curved shell. Other interesting work based on CUF [56-63] that could be extended to cover shells are needed.

The present two dimensional (2D) formulation is developed based on CUF with the inclusion of non-polynomial expansion function to study shells for the first time. This paper proposes different hybrid refined models (HRMs) including non-polynomial functions for the static analysis of simply supported laminated composite doubly-curved shell. The reported HRMs include polynomial, trigonometric, exponential and zig-zag functions. The kinematic models presented are adapted from the HRMs presented by Yarasca et al. [29-30]. The main contribution of this paper is to study the capabilities of these models for other types of transverse loading and study the effect of the curvature for the hybrid refined theories of Yarasca et al. [29-30]. The principal aims of this paper is to study the Yarasca' s HRMs considering the effect of curvature for different shell panels with constant curvature and also the capabilities of this model for other types of loading such as distributed, concentrated and hydrostatic. The highly coupled differential equations are solved via Navier type solutions.

This paper is organized as follows: Section 2 outlines the present unified formulation for shells; Section 3 present the analytical solution; the stress recovery from 3D elasticity equations is described in Section 4; the results and discussions are presented in Section 5. Finally, general conclusions are reported in Section 6.

2. Analytical Modelling of Composite Shells

The geometry and the coordinate system for a multilayered doubly-curved shell panel of "N_L" layers is given in Figure 1. The thickness of the panel is denoted as "*h*", the length as "*a*" and the width as "*b*". The coordinate system is considered as curvilinear, in which "α" and "β" are orthogonal. The radii of curvature "R_α" and "R_β" are considered as constant along the midsurface domain Ω_k . The integer *k* denotes the number of layer number from the shell-bottom.

2.1. Carrera Unified Formulation for Shells

According to CUF the displacement field of the shell can be written as follows:

$$\begin{cases} u = F_0 u_{\alpha 0} + F_1 u_{\alpha 1} + F_2 u_{\alpha 2} + F_3 u_{\alpha 3} + ... + F_N u_{\alpha N} \\ v = F_0 u_{\beta 0} + F_1 u_{\beta 1} + F_2 u_{\beta 2} + F_3 u_{\beta 3} + ... + F_N u_{\beta N} \\ w = F_0 u_{z 0} + F_1 u_{z 1} + F_2 u_{z 2} + F_3 u_{z 3} + ... + F_N u_{z N} \end{cases} \tag{1}$$

The displacement model according to CUF [47] is written in a compactness manner in term of Einstein's notation as:

$$\begin{aligned} &\delta u^k_{(\alpha,\beta,z)} = F_\tau(z)\delta u_\tau(\alpha,\beta); \\ &u^k_{(\alpha,\beta,z)} = F_s(z)u_s(\alpha,\beta); \tau,s = 0,1,2,3,...,N \\ &u^k_{(\alpha,\beta,z)} = F_s(z)u_s(\alpha,\beta); s = 0,1,2,3,...,N \end{aligned} \tag{2}$$

www.SID.ir

Archive of SID

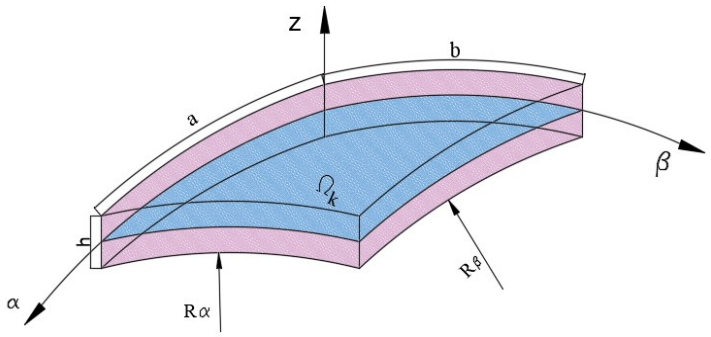

Fig. 1. Doubly-curved panel shell and curvilinear reference coordinate system.

where F_s and F_τ are the thickness functions and only depends on z. u^k is the displacement vector (u,v,w) whose components are the displacement in term of axis α,β and z, respectively. The displacement variable is denoted as u_s and its variation is described as u_τ. N represents the order of expansion in the thickness variation assumed for the displacement.

The ESL approach described that a multilayered shell can be described only as a single lamina. One of the most common expansion used in literature are the Maclaurin polynomials [46]. The thickness expansions are defined as $F_s = z^{\tau-1}$. The acronym for ESL is EDN, where *E* stands for Equivalent Single Layer Approach, *D* represents the PVD and *N* is defined as the order of the expansion. For example, if Maclaurin polynomials are considered, ED4 displacement vectors are given by:

$$\begin{aligned} u &= u_{\alpha 0} + z u_{\alpha 1} + z^2 u_{\alpha 2} + z^3 u_{\alpha 3} + z^4 u_{\alpha 4} \\ v &= u_{\beta 0} + z u_{\beta 1} + z^2 u_{\beta 2} + z^3 u_{\beta 3} + z^4 u_{\beta 4} \\ w &= u_{z 0} + z u_{z 1} + z^2 u_{z 2} + z^3 u_{z 3} + z^4 u_{z 4} \end{aligned} \tag{3}$$

Murakami [55] proposed adding a zig-zag function in the displacement field in order to approximate the thickness variation of the in-plane displacement. Murakami's Zig-Zag functions (MZZF) are defined as $M(z) = (-1)^k \zeta_k$. The acronym referring to Maclaurin polynomial enhanced with a MZZF is EDZN, where *E* is referred to ESL approach, *D* is referred to PVD, *Z* stands for the inclusion of a MZZF and *N* is the order of expansion. For example EDZN4 is denoted as:

$$\begin{aligned} u &= u_{\alpha 0} + z u_{\alpha 1} + z^2 u_{\alpha 2} + z^3 u_{\alpha 3} + z^4 u_{\alpha 4} + (-1)^k \zeta_k u_{\alpha 5} \\ v &= u_{\beta 0} + z u_{\beta 1} + z^2 u_{\beta 2} + z^3 u_{\beta 3} + z^4 u_{\beta 4} + (-1)^k \zeta_k u_{\beta 5} \\ w &= u_{z 0} + z u_{z 1} + z^2 u_{z 2} + z^3 u_{z 3} + z^4 u_{z 4} + (-1)^k \zeta_k u_{z 5} \end{aligned} \tag{4}$$

where $\zeta_k = 2\times(z - 0.5(z_{k+1} - z_k))/h^k$ is a non-dimensional layer coordinates, h^k is the thickness of the *k*-layer and z_{k+1} and z_k are the top and the bottom of the z coordinates at each *k*-layer. The main objective of CUF is to write any higher order models with any desired order and using several types of thickness expansions $F_\tau(z)$. In this context, several researchers [31, 32, 26-29] had formulated different non-polynomial models based on CUF for plates and shells.

The presented paper investigates the influence of different trigonometrical, exponential and zig zag shear strain shape functions in ESL models. The displacement field proposed for this paper is based on a selection of thickness functions proposed by Filippi et al. [27] which were used by Yarasca et al. [30] for employing Axiomatic/Asymptotic method and genetic algorithms for creating different Best Theory Diagrams (BTDs). The models proposed by Filippi et al. [27] and Yarasca et al. [30] are presented for plates, however this paper used this refined models in order to study the capabilities to the effect of the curvature. The complete displacement field is based on 17 thickness functions which are 5 Maclaurin functions, the zig-zag function and 8 trigonometrical terms and 4 exponential terms. The acronym used for this model is EDZ17. The expansion along β axis is denoted as:

$$\begin{aligned} v &= u_{\beta 0} + z u_{\beta 1} + z^2 u_{\beta 2} + z^3 u_{\beta 3} + z^4 u_{\beta 4} + (-1)^k \zeta_k u_{\beta 5} + \sin\left(\frac{\pi z}{h}\right) u_{\beta 6} + \sin\left(\frac{2\pi z}{h}\right) u_{\beta 7} + \sin\left(\frac{3\pi z}{h}\right) u_{\beta 8} + \sin\left(\frac{4\pi z}{h}\right) u_{\beta 9} \\ &+ \cos\left(\frac{\pi z}{h}\right) u_{\beta 10} + \cos\left(\frac{2\pi z}{h}\right) u_{\beta 11} + \cos\left(\frac{3\pi z}{h}\right) u_{\beta 12} + \cos\left(\frac{4\pi z}{h}\right) u_{\beta 13} + e^{\frac{z}{h}} u_{\beta 14} + e^{\frac{2z}{h}} u_{\beta 15} + e^{\frac{3z}{h}} u_{\beta 16} + e^{\frac{4z}{h}} u_{\beta 17} \end{aligned} \tag{5}$$

where h is the thickness of the shell. Refined models are defined as *N* hybrid refined models (*N* HRM), where the *N* notation is the number of the variables in the model. In this context, some hybrid refined models (*N* HRM) are reported in Table 1. Layerwise (LW) approach described a multilayered shell layer by layer. The displacement field in term of LW approach [47, 48] is presented in what follows:

$$u = F_s(z) u_s(\alpha,\beta) = F_t(\zeta_k) u_t^k + F_b(\zeta_k) u_b^k + F_r(\zeta_k) u_r^k, s = t,b,r, r = 2,3,...,N \tag{6}$$

www.SID.ir

Archive of SID

Table 1. Hybrid refined models (HRM).

Model	Disp.	z^N					$(-1)^k \varsigma_k$	$\sin(\frac{N\pi}{h}z)$			$\cos(\frac{N\pi}{h}z)$		$e^{\frac{Nz}{h}}$		
		0	1	2	3	4	--	1	2	3	1	3	1	2	3
12 HRM	u	e	e	e	e	-	e	-	-	-	-	-	-	-	-
	v	e	e	-	e	-	-	-	-	-	-	-	-	-	-
	w	e	e	e	-	e	-	-	-	-	-	-	-	-	-
15 HRM	u	e	e	e	e	-	e	e	-	-	-	-	-	-	-
	v	e	e	-	e	-	e	-	e	-	-	-	-	-	-
	w	e	e	e	-	e	-	-	-	-	-	-	-	-	-
16 HRM	u	e	e	-	e	-	e	-	-	-	e	-	e	-	-
	v	e	e	-	-	-	e	-	-	-	e	-	e	-	e
	w	e	e	-	-	-	e	-	-	-	-	-	e	-	-
18 HRM	u	e	e	e	e	-	e	e	e	-	-	-	-	-	-
	v	e	e	-	e	-	e	e	e	-	-	-	-	-	-
	w	e	e	e	-	e	-	-	-	-	e	-	-	-	-
20 HRM	u	e	e	-	-	-	e	-	e	-	-	-	e	-	e
	V	e	e	-	-	-	e	e	e	-	-	-	e	-	e
	W	e	e	-	-	e	e	-	-	e	-	-	e	-	-
21 HRM	U	e	e	e	e	-	e	e	e	-	-	-	-	-	-
	V	e	e	-	e	-	e	e	e	-	-	-	e	e	-
	W	e	e	e	-	e	-	-	-	-	e	e	-	-	-

The subscript b and t denoted the bottom and the top surface of the shell. The order of expansion is defined as N. The thickness functions F_τ are defined as:

$$F_t = \frac{P_0 + P_1}{2}, F_b = \frac{P_0 - P_1}{2}, F_r = P_r - P_{r-2}, r = 2,3,...,N \tag{7}$$

where $P_j = P_j(\zeta_k)$ are defined as Legendre's polynomials of j order and are presented as follows:

$$P_0 = 1, P_1 = \zeta_k, P_2 = \frac{3\zeta_k{}^2 - 1}{2}, P_3 = \frac{5\zeta_k{}^3 - 3\zeta_k}{2}, P_3 = \frac{35\zeta_k{}^4 - 30\zeta_k{}^2 + 3}{8} \tag{8}$$

The acronym for Layer-Wise approach is denoted as LDN, where L denoted Layer-wise approach, D stands for Principle of Virtual Displacement and N is the order of expansion.

2.2. Elastic stress-strain relations

The stress (σ^k) and strain (ε^k) are developed as matrix for each kth -layer level:

$$\begin{aligned} \sigma_p^k &= \begin{bmatrix} \sigma_{\alpha\alpha}^k & \sigma_{\beta\beta}^k & \tau_{\alpha\beta}^k \end{bmatrix}^T, \sigma_n^k = \begin{bmatrix} \tau_{\alpha z}^k & \tau_{\beta z}^k & \sigma_{zz}^k \end{bmatrix}^T, \\ \varepsilon_p^k &= \begin{bmatrix} \varepsilon_{\alpha\alpha}^k & \varepsilon_{\beta\beta}^k & \gamma_{\alpha\beta}^k \end{bmatrix}^T, \xi_n^k = \begin{bmatrix} \gamma_{\alpha z}^k & \gamma_{\beta z}^k & \varepsilon_{zz}^k \end{bmatrix}^T \end{aligned} \tag{9}$$

with the subscripted p represented the in-plane component and n referred to the out-plane component, the strain-displacement linear relationship is given by:

$$\varepsilon_p^k = (D_p^k + A_p^k)u^k, \varepsilon_n^k = D_n^k u^k = (D_{np}^k + D_{nz}^k - A_n^k)u^k$$

$$D_p^k = \begin{pmatrix} \frac{1}{H_\alpha^k}\frac{\partial}{\partial\alpha} & 0 & 0 \\ 0 & \frac{1}{H_\beta^k}\frac{\partial}{\partial\beta} & 0 \\ \frac{1}{H_\beta^k}\frac{\partial}{\partial\beta} & \frac{1}{H_\alpha^k}\frac{\partial}{\partial\alpha} & 0 \end{pmatrix}, D_{np}^k = \begin{pmatrix} 0 & 0 & \frac{1}{H_\alpha^k}\frac{\partial}{\partial\alpha} \\ 0 & 0 & \frac{1}{H_\beta^k}\frac{\partial}{\partial\beta} \\ 0 & 0 & 0 \end{pmatrix}, D_{nz}^k = \begin{pmatrix} \frac{\partial}{\partial z} & 0 & 0 \\ 0 & \frac{\partial}{\partial z} & 0 \\ 0 & 0 & \frac{\partial}{\partial z} \end{pmatrix}, \tag{10}$$

$$A_p^k = \begin{pmatrix} 0 & 0 & \frac{1}{H_\alpha^k R_\alpha^k} \\ 0 & 0 & \frac{1}{H_\beta^k R_\beta^k} \\ 0 & 0 & 0 \end{pmatrix}, A_n^k = \begin{pmatrix} \frac{1}{H_\alpha^k R_\alpha^k} & 0 & 0 \\ 0 & \frac{1}{H_\beta^k R_\beta^k} & 0 \\ 0 & 0 & 0 \end{pmatrix}$$

www.SID.ir

Archive of SID

where H_α^k and H_β^k are the metric coefficients which as denoted as follow:

$$H_\alpha^k = A^k(1+\frac{z}{R_\alpha^k}), H_\beta^k = B^k(1+\frac{z}{R_\beta^k}) \tag{11}$$

in which A^k and B^k are the Lame parameters, as this paper only deals with shells with constant radii of curvature, this parameters are considered as $A^k = B^k = 1$. It is remarkable that more complicated middle surface needs a completely review on differential geometry which can be seen in papers by Viola et al. [40, 41]. The metric coefficients H_α^k and H_β^k are calculated in two different manners [49].

The stress-strain relations in material coordinates of the kth-layer:

$$\begin{bmatrix}\sigma_{\alpha\alpha}^k\\ \sigma_{\beta\beta}^k\\ \tau_{\alpha\beta}^k\\ \tau_{\alpha z}^k\\ \tau_{\beta z}^k\\ \sigma_{zz}^k\end{bmatrix} = \begin{bmatrix} C_{11}^k & C_{12}^k & C_{16}^k & 0 & 0 & C_{13}^k\\ C_{12}^k & C_{22}^k & C_{26}^k & 0 & 0 & C_{23}^k\\ C_{16}^k & C_{26}^k & C_{33}^k & 0 & 0 & C_{36}^k\\ 0 & 0 & 0 & C_{55}^k & C_{45}^k & 0\\ 0 & 0 & 0 & C_{45}^k & C_{44}^k & 0\\ C_{13}^k & C_{23}^k & C_{36}^k & 0 & 0 & C_{33}^k\end{bmatrix}\begin{bmatrix}\varepsilon_{\alpha\alpha}^k\\ \varepsilon_{\beta\beta}^k\\ \gamma_{\alpha\beta}^k\\ \gamma_{\alpha z}^k\\ \gamma_{\beta z}^k\\ \varepsilon_{zz}^k\end{bmatrix} \tag{12}$$

The calculation of the materials coefficients C_{ij}^k (see Refs. [45] and [46]), which depends on young modulus E_1, E_2, E_3, poisson coefficients $\nu_{12}, \nu_{13}, \nu_{23}$, shear modulus G_{12}, G_{13}, G_{23} is reported as follows:

$$\begin{aligned}
&\frac{\nu_{ij}^k}{E_i^k} = \frac{\nu_{ji}^k}{E_j^k}; i, j = 1,2,3\\
&C_{11}^k = \frac{1-\nu_{23}^k\nu_{32}^k}{E_2^k E_3^k \Delta}, C_{12}^k = \frac{\nu_{21}^k+\nu_{31}^k\nu_{23}^k}{E_2^k E_3^k \Delta}, C_{13}^k = \frac{\nu_{31}^k+\nu_{21}^k\nu_{32}^k}{E_2^k E_3^k \Delta},\\
&C_{22}^k = \frac{1-\nu_{13}^k\nu_{31}^k}{E_1^k E_3^k \Delta}, C_{12}^k = \frac{\nu_{32}^k+\nu_{12}^k\nu_{31}^k}{E_1^k E_3^k \Delta}, C_{33}^k = \frac{1-\nu_{12}^k\nu_{21}^k}{E_1^k E_2^k \Delta},\\
&C_{44}^k = G_{23}^k, C_{55}^k = G_{13}^k, C_{66}^k = G_{12}^k,\\
&\Delta = \frac{1-\nu_{12}^k\nu_{21}^k-\nu_{23}^k\nu_{32}^k-\nu_{31}^k\nu_{13}^k-2\nu_{13}^k\nu_{21}^k\nu_{32}^k}{E_1^k E_2^k E_3^k}
\end{aligned} \tag{13}$$

The Equation (12) can be expressed in a simplify format:

$$\sigma_m^k = C\,\varepsilon_m^k \tag{14}$$

where σ_m^k, ε_m^k and C are written in term of material coordinates. The stresses and material coefficients must be in written in terms of curvilinear coordinates and this is achieved by using the next rotation matrix:

$$L^k = \begin{bmatrix} \cos^2\theta^k & \sin^2\theta^k & -\sin 2\theta^k & 0 & 0 & 0\\ \sin^2\theta^k & \cos^2\theta^k & \sin 2\theta^k & 0 & 0 & 0\\ \sin\theta^k\cos\theta^k & -\sin\theta^k\cos\theta^k & \cos 2\theta^k & 0 & 0 & 0\\ 0 & 0 & 0 & \cos\theta^k & -\sin\theta^k & 0\\ 0 & 0 & 0 & \sin\theta^k & \cos\theta^k & 0\\ 0 & 0 & 0 & 0 & 0 & 1\end{bmatrix} \tag{15a-c}$$

$$\sigma^k = L^k\sigma_m^k$$

$$\varepsilon_m^k = L^{k^T}\varepsilon^k$$

where θ^k is the angle between the material coordinates and the curvilinear shell coordinates. A shallow shell with different layers and angles orientation (θ^k) is presented in Figure 2. By replacing Equations (15a) and (14) in Equation (15b) and (15c), the following relation is obtained:

$$\sigma^k = L^k C L^{k^T}\varepsilon^k \tag{16}$$

The following notation can be adopted:

$$\tilde{C} = L^k C L^{k^T} \tag{17}$$

www.SID.ir

Archive of SID

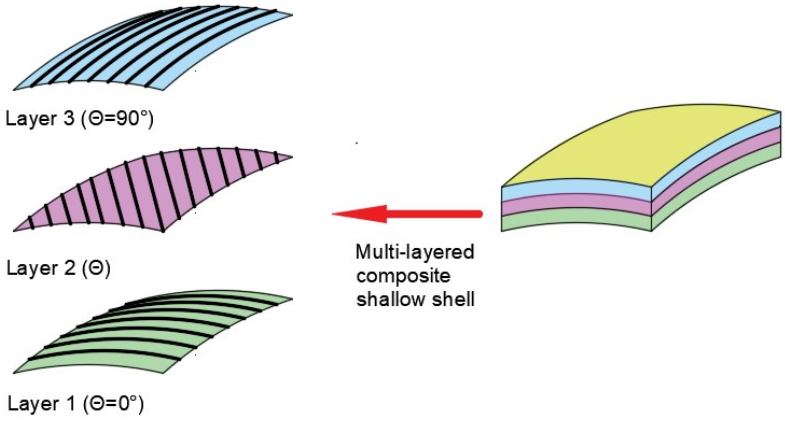

Fig. 2. Multilayered composite shell with different rotation angles in its layer (θ^k) .

Note that Equation (18) is simplified by using Equations (16) and (17), therefore the stresses and strains are written in term of shell coordinate:

$$\sigma^k = \tilde{C}^k \varepsilon^k \tag{18}$$

According to Equations (9a-d), the stress components for a generic k layer are denoted as:

$$\begin{aligned} \sigma_p^k &= C_{pp}^k \varepsilon_p^k + C_{pn}^k \varepsilon_n^k \\ \sigma_n^k &= C_{np}^k \varepsilon_p^k + C_{nn}^k \varepsilon_n^k \end{aligned} \tag{19a-b}$$

where C_{pp}^k , C_{pn}^k , C_{np}^k and C_{nn}^k are:

$$\begin{aligned} C_{pp}^k &= \begin{bmatrix} \tilde{C}_{11}^k & \tilde{C}_{12}^k & \tilde{C}_{16}^k \\ \tilde{C}_{12}^k & \tilde{C}_{22}^k & \tilde{C}_{26}^k \\ \tilde{C}_{16}^k & \tilde{C}_{26}^k & \tilde{C}_{66}^k \end{bmatrix}, C_{pp}^k = \begin{bmatrix} 0 & 0 & \tilde{C}_{13}^k \\ 0 & 0 & \tilde{C}_{23}^k \\ 0 & 0 & \tilde{C}_{36}^k \end{bmatrix}, \\ C_{pp}^k &= \begin{bmatrix} 0 & 0 & 0 \\ 0 & 0 & 0 \\ \tilde{C}_{13}^k & \tilde{C}_{23}^k & \tilde{C}_{36}^k \end{bmatrix}, C_{pp}^k = \begin{bmatrix} \tilde{C}_{55}^k & \tilde{C}_{45}^k & 0 \\ \tilde{C}_{45}^k & \tilde{C}_{44}^k & 0 \\ 0 & 0 & \tilde{C}_{66}^k \end{bmatrix} \end{aligned} \tag{20a-d}$$

2.3. Principle of virtual work

The governing equations are calculated via the Principle of Virtual Displacement (PVD), which states that:

$$\delta L_{\text{int}} = \delta L_{ext} \tag{21}$$

where δL_{int} is the virtual variation of the internal work and δL_{ext} is the virtual variation of work created by external loading. The PVD for multilayered doubly-curved shell is presented as:

$$\sum_{k=1}^{N_l} \int_{\Omega_k} \int_{A_k} \{\delta {\varepsilon_p^k}^T \sigma_p^k + \delta {\varepsilon_n^k}^T \sigma_n^k\} H_\alpha^k H_\beta^k d\Omega_k dz = \sum_{k=1}^{N_l} \int_{\Omega_k} \int_{A_k} \{\delta {u^k}^T p^k\} H_\alpha^k H_\beta^k d\Omega_k dz \tag{22}$$

where Ω_k and A_k represents the integration domains in plane and the thickness direction, respectively. p^k is the mechanical load applied at a certain k layer. Equations (15a-b) and (24a-b) are replaced into Equation (22):

$$\begin{aligned} &\sum_{k=1}^{N_l} \int_{\Omega_k} \int_{A_k} \{\left(\left(D_p^k + A_p^k\right)\delta u^k\right)^T \left(C_{pp}^k \left(D_p^k + A_p^k\right) u^k + C_{pn}^k \left(D_{np}^k + D_{nz}^k - A_n^k\right) u^k\right) + \\ &\left(\left(D_{np}^k + D_{nz}^k - A_n^k\right)\delta u^k\right)^T \left(C_{np}^k \left(D_p^k + A_p^k\right) u^k + C_{nn}^k \left(D_{np}^k + D_{nz}^k - A_n^k\right) u^k\right)\} H_\alpha^k H_\beta^k d\Omega_k dz = \\ &\sum_{k=1}^{N_l} \int_{\Omega_k} \int_{A_k} \{\delta {u^k}^T p^k\} H_\alpha^k H_\beta^k d\Omega_k dz \end{aligned} \tag{23}$$

The displacement field presented in Equation (2) is replaced in Equation (23):

www.SID.ir

Archive of SID

$$\sum_{k=1}^{N_l}\int_{\Omega_k}\int_{A_k}\{\left(\left(D_p^k+A_p^k\right)F_\tau\delta u_\tau^k\right)^T\left(C_{pp}^k\left(D_p^k+A_p^k\right)F_s u_s^k+C_{pn}^k\left(D_{np}^k+D_{nz}^k-A_n^k\right)F_s u_s^k\right)+$$
$$\left(\left(D_{np}^k+D_{nz}^k-A_n^k\right)F_\tau\delta u_\tau^k\right)^T\left(C_{np}^k\left(D_p^k+A_p^k\right)F_s u_s^k+C_{nn}^k\left(D_{np}^k+D_{nz}^k-A_n^k\right)F_s u_s^k\right)\}H_\alpha^k H_\beta^k d\Omega_k dz = \tag{24}$$
$$\sum_{k=1}^{N_l}\int_{\Omega_k}\int_{A_k}\{\delta u_\tau^{kT} p^k\}F_\tau H_\alpha^k H_\beta^k d\Omega_k dz$$

The subscript z represents partial derivatives respect to z. The integration by parts is presented as follows:

$$\int_{\Omega_k}(D_\Omega^k\delta a^k)^T = -\int_{\Omega_k}\delta a^{kT}((D_\Omega^{kT})a^k)+\int_{\Gamma_k}\delta a^{kT}(I_\Omega^k)a^k d\Gamma_k \tag{25}$$

By applicating the integration by part formulation (Equation (25)) into Equation (24), the boundary and internal governing equations are obtained:

$$\sum_{k=1}^{N_l}\int_{\Omega_k}\delta u_\tau^{kT}(K_{uu}^{k\tau s})u_s^k d\Omega_k+\int_{T_k}\delta u_\tau^{kT}(\Pi_{uu}^{k\tau s})u_s^k d\Omega_k=\sum_{k=1}^{N_l}\int_{\Omega_k}\left\{(\delta u_\tau^{kT})P_{u\tau}^k\right\}u_s^k d\Omega_k \tag{26}$$

where $K_{uu}^{k\tau s}$ is the stiffness matrix of the fundamental nuclei, $P_{u\tau}^k$ is the external mechanical load and $\Pi_{uu}^{k\tau s}$ represents the boundary conditions. The terms are expressed as follows:

$$K_{uu}^{k\tau s}=\int_{A_k}\{(-F_\tau D_p^k+F_\tau A_p^k)^T(C_{pp}^k(F_s D_p^k+F_s A_p^k)+C_{pn}^k(F_s D_{np}^k+F_{s,z}-F_s A_n^k))+$$
$$(F_\tau D_{np}^k+F_{\tau,z}-F_\tau A_n^k)^T(C_{np}^k(F_s D_p^k+F_s A_p^k)+C_{nn}^k(F_s D_{np}^k+F_{s,z}-F_s A_n^k))\}H_\alpha^k H_\beta^k dz$$
$$\Pi_{uu}^{k\tau s}=\int_{A_k}\{(I_p^k)^T(F_\tau C_{pp}^k(F_s D_p^k+F_s A_p^k)+F_\tau C_{pn}^k(F_s D_{np}^k+F_{s,z}-F_s A_n^k))+$$
$$(I_{np}^k)^T(F_\tau C_{np}^k(F_s D_p^k+F_s A_p^k)+F_\tau C_{nn}^k(F_s D_{np}^k+F_{s,z}-F_s A_n^k))\}H_\alpha^k H_\beta^k dz$$
$$P_{u\tau}^k=\left[0\quad 0\quad \bar{F}_\tau q_{z(\alpha,\beta)}\right],\bar{F}_\tau=F_\tau\big|_{z=h/2}H_\alpha^k\big|_{z=h/2}H_\beta^k\big|_{z=h/2} \tag{27}$$
$$I_p^k=\begin{bmatrix}\frac{1}{H_\alpha^k} & 0 & 0\\ 0 & \frac{1}{H_\beta^k} & 0\\ \frac{1}{H_\beta^k} & \frac{1}{H_\alpha^k} & 0\end{bmatrix},I_{np}^k=\begin{bmatrix}0 & 0 & \frac{1}{H_\alpha^k}\\ 0 & 0 & \frac{1}{H_\beta^k}\\ 0 & 0 & 0\end{bmatrix}$$

The equilibrium and compatibility equations are

$$(\delta u_\tau^k)^T:K_{uu}^{k\tau s}u_s^k=P_{u\tau}^k \tag{28}$$

3. Analytical Solution

The numerical results were obtained via the Navier closed-form solution for simply supported orthotropic panels. The following properties hold:

$$C_{16}^k=C_{26}^k=C_{36}^k=C_{45}^k=0 \tag{29}$$

The displacement expressed as a summation of harmonics:

$$u_{\alpha_s}^k=\sum_{m,n}U_{\alpha_s}^k\cos\left(\frac{m\pi}{a}\alpha\right)\sin\left(\frac{n\pi}{b}\beta\right)$$
$$u_{\beta_s}^k=\sum_{m,n}U_{\beta_s}^k\sin\left(\frac{m\pi}{a}\alpha\right)\cos\left(\frac{n\pi}{b}\beta\right) \tag{30}$$
$$u_{z_s}^k=\sum_{m,n}U_{z_s}^k\sin\left(\frac{m\pi}{a}\alpha\right)\sin\left(\frac{n\pi}{b}\beta\right)$$

where m and n are the number of waves and $U_{\alpha_s}^k$, $U_{\beta_s}^k$ and $U_{z_s}^k$ are related to the amplitudes of the Fourier series displacement.

www.SID.ir

Archive of SID

3.1. External mechanical load

The transverse external mechanical load are also expressed in terms summation of harmonics:

$$p_{z_s}^k = \sum_{m,n} P_{mn}^k \sin\left(\frac{m\pi}{a}\alpha\right)\sin\left(\frac{n\pi}{b}\beta\right) \tag{31}$$

The load coefficient are calculated as follows:

$$P_{mn}^k = \frac{4}{ab}\int_0^b\int_0^a p_{z_s}^k \sin\left(\frac{m\pi}{a}\alpha\right)\sin\left(\frac{n\pi}{b}\beta\right)d\alpha d\beta \tag{32}$$

The coefficient must be adapted to be applied in different types of mechanical loadings. The loads considered are shown in Figure 3.

3.2. Bi-Sinusoidal load

A simply supported shell panel subjected to a bi-sinusoidal load on the surface $z = h/2$ acting on z direction is considered. The load are expressed as:

$$p_{z_s}^k = P_z \sin\left(\frac{m\pi}{a}\alpha\right)\sin\left(\frac{n\pi}{b}\beta\right) \tag{33}$$

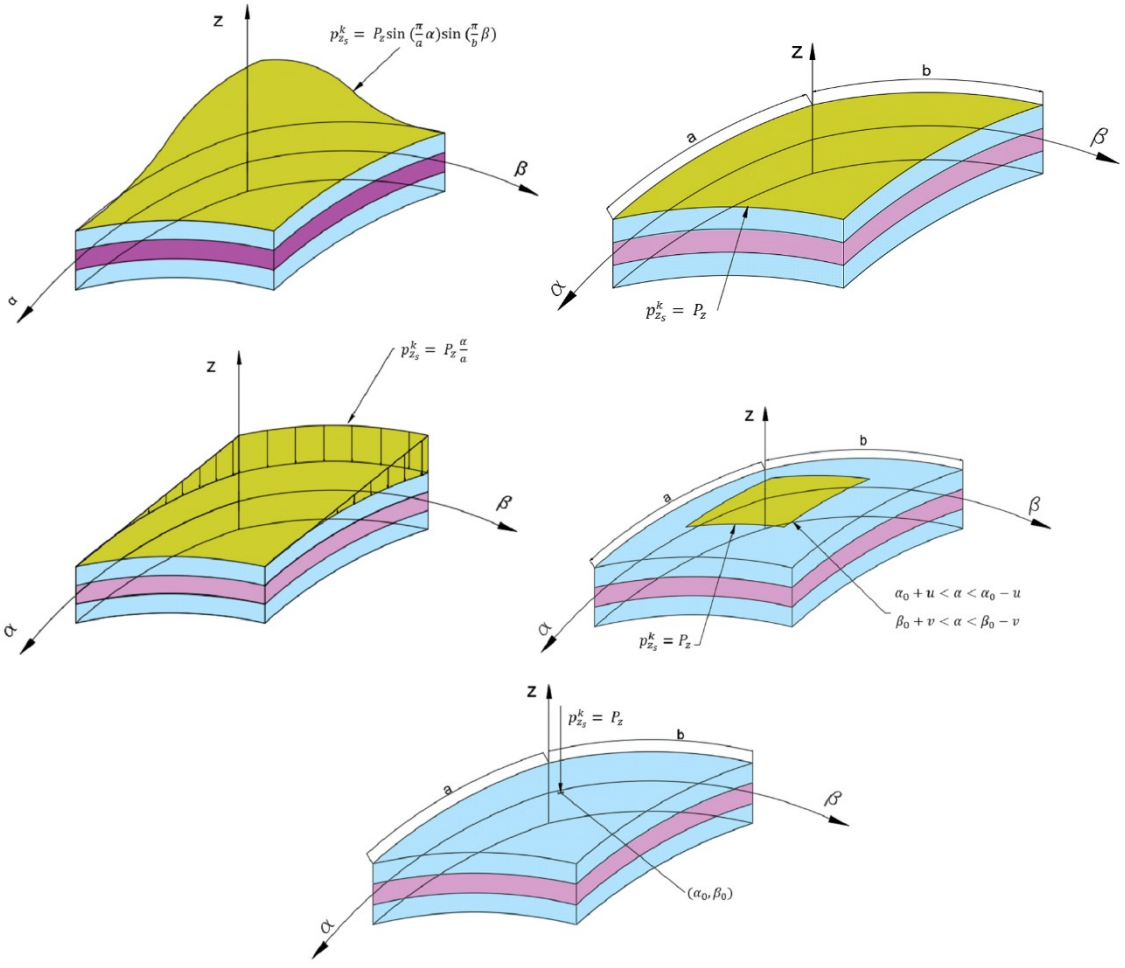

Fig. 3. Doubly-curved panel shell subjected to different types of transverse mechanical loading (bi-sinusoidal, distributed uniform, patch, hydrostatic pressure and point load).

3.3. Uniformly distributed load

A simply supported shell panel subjected to a uniformly distributed load on the surface $z = h/2$ acting on z direction is considered. The load coefficients are expressed as:

www.SID.ir

$$P_{mn}^{k}=\begin{cases}\dfrac{16P_z}{\pi^2 mn},\ \text{for}\{m,n\}=1,3,5,7,...\\ 0,\ \text{for}\{m,n\}=2,4,6,8,...\end{cases} \tag{34}$$

3.4. Hydrostatic load

A simply supported shell panel subjected to a linearly varying load $p_{z_s(\alpha)}^{k}=P_z\alpha/a$ acting on the surface $z=h/2$ acting on z direction is considered. The load coefficients are expressed as:

$$P_{mn}^{k}=\begin{cases}\dfrac{-8P_z}{\pi^2 mn}\cos(m\pi),\ \text{for}\{m,n\}=1,3,5,7,...\\ 0,\ \text{for}\{m,n\}=2,4,6,8,...\end{cases} \tag{35}$$

3.5. Patch load

A simply supported shell panel subjected to a constant load $p_{z_s}^{k}=P_z$ at the top of the shell in the domain of $\alpha_0-u\le\alpha\le\alpha_0+u$ and $\beta_0-v\le\beta\le\beta_0+v$ is considered. The load coefficients are calculated as:

$$P_{mn}^{k}=\frac{16P_z}{\pi^2 mn}\sin\left(\frac{m\pi\alpha_0}{a}\right)\sin\left(\frac{m\pi u}{a}\right)\sin\left(\frac{m\pi\beta_0}{b}\right)\sin\left(\frac{m\pi v}{b}\right),\ \text{for}\{m,n\}=1,2,3,4,... \tag{36}$$

3.6. Point load

A simply supported shell panel subjected to a concentrated load $p_{z_s}^{k}=P_z$ oriented at (α_0,β_0) is considered. The load coefficients are expressed as:

$$P_{mn}^{k}=\frac{4P_z}{ab}\sin\left(\frac{m\pi\alpha_0}{a}\right)\sin\left(\frac{m\pi\beta_0}{b}\right),\ \text{for}\{m,n\}=1,2,3,4,... \tag{37}$$

4. Stress Recovery from 3D Elasticity Equilibrium Equations for 2D Shell Model

Static problems of doubly curved shells with constant radii of curvature are solved using a 2D theory with unknown variables at the mid-surface. This paper presents a simplified model of 3D elasticity theories with the assumptions of the displacement imposed by the displacement field presented in Equations (1). The presented refined models can capture the real behavior of shell structures for displacement and in-plane stresses. However, a refinement is need for transverse shear stresses and transverse normal stress. The 3D elasticity are valid for solving problems of shells with simply supported boundary conditions. The shear stresses and their derivatives are used for replacing into the 3D elasticity equations in order to calculate the out-plane stresses.

The differential equations are solved analytically for the out-plane stresses, as follows:

$$\begin{aligned}
\tau_{\alpha z}^{k}&=\frac{c_1^k}{(R_\alpha^k H_\alpha^k)^2 R_\beta^k H_\beta^k}-\frac{1}{(H_\alpha^k)^2 H_\beta^k}\left(\int\left((H_\alpha^k)^2\frac{\partial\tau_{\alpha\beta}^k}{\partial\beta}+H_\alpha^k H_\beta^k\frac{\partial_{\alpha\alpha}^k}{\partial\alpha}\right)dz\right)\\
\tau_{\beta z}^{k}&=\frac{c_2^k}{(R_\beta^k H_\beta^k)^2 R_\alpha^k H_\alpha^k}-\frac{1}{(H_\beta^k)^2 H_\alpha^k}\left(\int\left((H_\beta^k)^2\frac{\partial\tau_{\alpha\beta}^k}{\partial\alpha}+H_\alpha^k H_\beta^k\frac{\partial_{\beta\beta}^k}{\partial\beta}\right)dz\right)\\
\sigma_{zz}^{k}&=\frac{c_3^k}{R_\beta^k H_\beta^k R_\alpha^k H_\alpha^k}-\frac{1}{H_\beta^k H_\alpha^k}\left(\int\left(\frac{H_\beta^k}{R_\alpha^k}\sigma_{\alpha\alpha}^k+\frac{H_\alpha^k}{R_\beta^k}\sigma_{\beta\beta}^k-H_\beta^k\frac{\partial\tau_{\alpha z}^k}{\partial\alpha}-H_\alpha^k\frac{\partial\tau_{\beta z}^k}{\partial\beta}\right)dz\right)
\end{aligned} \tag{38a-c}$$

where c_1^k, c_2^k, c_3^k are two constants for the transverse shear stresses $\tau_{\alpha z}^k$, $\tau_{\beta z}^k$ and transverse normal stress σ_{zz}^k, respectively. The presented constant must satisfy the zero shear strain condition at the bottom and the top of the shell structure and interlaminar continuity. The constant for the transverse normal stress and must satisfy interlaminar continuity and the boundary condition on the top. Some integrals presented in Equations (38a-c) could not be solved analytically, so an approximate solution using Taylor series is adopted. The equations (38a-c) are valid for doubly curved with constant radii of curvature; however for specific cases such as cylindrical panels and plates the presented strategy can be simplify by avoiding the corresponding radii of curvature.

www.SID.ir

Archive of SID

5. Results and Discussions

In the present section, some results of the static analysis of composite doubly-curved shell panels are presented. The boundary conditions are considered as simply supported. The geometry data is considered as: $a = b = 1$ and $R_\alpha = R_\beta = R$. Different side-to-thickness (a/h) and curvature-radius-to-side (R/a) ratios are considered as parameters. The first case is related to a laminated doubly-curvature panel with the stacking sequence 0°/90°/0° subjected to different types of transverse loadings: bi-sinusoidal, distributed uniform, patch, hydrostatic and point loading. Some results are compared with different HSDTs [10-13, 38, 50, 52-54] available in the literature. The second case is a benchmark solution of two lamina, subjected to bi-sinusoidal loading. The original problem was presented by Demasi [18] for plates and it is used for the first time to doubly-curved panels in this paper. It should be taken into account that equilibrium equations is adopted for the 2D models in order to calculate of the transverse shear and normal stresses. The in-plane stresses are calculated directly for constitutive equations and out-plane stresses are calculated by the stress recovery procedure reported in Section 5.

5.1. Case 1

The mechanical properties of each layer were reported by Reddy and Liu [12]:

$$E_1 = 25E_2, G_{12} = G_{13} = 0.5E_2, G_{23} = 0.2E_2, \nu_{12} = \nu_{13} = 0.25 \tag{39}$$

In this paper, the transverse displacement u_z and transverse normal stress σ_{zz} is evaluated at (a/2, b/2, 0). The normal stress $\sigma_{\alpha\alpha}$ is evaluated at (a/2, b/2, h/2). The transverse shear stress $\tau_{\alpha z}$ and $\tau_{\beta z}$ are computed at (0, b/2, 0) and (a/2, 0, 0), respectively. Shear in-plane stress $\tau_{\alpha\beta}$ is evaluated at (0, 0, h/2). The results are presented with the following normalizations:

$$\bar{w} = \frac{10^3 E_2 h^3 u_z}{P_z a^4}, (\bar{\sigma}_{\alpha\alpha}, \bar{\tau}_{\alpha\beta}, \bar{\tau}_{\alpha z}, \bar{\tau}_{\beta z}) = \frac{h^2}{a^2 P_z}(\sigma_{\alpha\alpha}, \tau_{\alpha\beta}, \tau_{\alpha z}, \tau_{\beta z}), \bar{\sigma}_{zz} = \frac{1}{P_z}\sigma_{zz} \tag{40}$$

In all cases, the considered amplitude of the load P_z is considered as 1 kPa. In the 2D shell model, the refined models are selected from the work of Yarasca et al. [30]. The extracted theories are the ones with the lowest percentage of error in the Pareto Fronts for a cross-ply 0°/90°/0° composite simply supported plate subjected to a bi-sinusoidal load at the top. The authors [30] demonstrated that in in refined models for 0°/90°/0° the trigonometric terms are more effective than the exponential ones. The principal objective of selecting this HRMs is to study the capabilities of such plate theories in holding the effect of the curvature and other type of transverse loadings such as: distributed uniform, patch, hydrostatic and point.

5.1.1. Bi-sinusoidal load

A shell subjected to bi-sinusoidal loading with $m = n = 1$ and $P_z = 1kPa$ applied at the top (see Figure 3). Results on transverse displacement for thick panel $(a/h = 5)$ are reported in Table 2. As the number of terms of the HRM increased, the error percentage is less compared with a three-dimensional numerical solution reported by Huang [10]. It is noted that the error for the hybrid model is less than 0.7% while the full polynomial model ED4 is around 5.44% for deep shells. The reported results for plates of HRM are around 0.40%.

Table 2. Dimensionless center deflection $\bar{w}$ for 0°/90°/0°, $a/h = 5$ shell under bi-sinusoidal loading.

R/a	2	Diff (%)	5	Diff (%)	Plate	Diff (%)
3D Elasticity [10]	1.4820	--	1.5490	--	1.5250	--
Huang [10]	1.4200	4.18	1.4610	5.68	1.4420	5.44
Shu [11]	1.4820	0.00	1.5460	0.19	--	--
Tornabene et al. [38]	1.4830	0.07	1.5455	0.23	--	--
LD4	1.4824	0.03	1.5494	0.03	1.5253	0.02
ED4	1.4038	5.28	1.4564	5.98	1.4316	6.12
12 HRM	1.4721	0.67	1.5425	0.42	1.5192	0.38
15 HRM	1.4757	0.43	1.5469	0.14	1.5237	0.09
18 HRM	1.4765	0.37	1.5479	0.07	1.5247	0.02
21 HRM	1.4807	0.09	1.5486	0.03	1.5247	0.02

The results for transverse deformation and stresses for a moderate thick shell $(a/h = 10)$ and different curvature-radius-to-size (R/a) ratios are reported in Table 3. In all cases, the normalized transverse displacements calculated with HRMs model present a lower numerical value than the ones calculated with LD4. The error is calculated from LD4 solution. In all cases for $\bar{w}$, the error predicted by the HRMs are less than ED4. The results demonstrated that all the HRM presents almost the same accuracy. The error of transverse displacement tends to increase as the ratio (R/a) decrease. The error of the normal stress is less than 0.7% in all the curvature-radius-to-size ratios presented while ED4 is around 1.4%. The maximum error reported by the HRM for transverse shear stresses are 0.10% and 0.28% for $\bar{\tau}_{\alpha z}$ and $\bar{\tau}_{\beta z}$, respectively while the ED4 presented a maximum error of 2.76% and 3.84%. The results of transverse normal stress suggested that the error increased as the (R/a) ratio decreased. Figure 4 shows the dimensionless displacement $\bar{w}$ and the stresses $\bar{\sigma}_{\alpha\alpha}, \bar{\sigma}_{\alpha\beta}, \bar{\sigma}_{\alpha z}, \bar{\sigma}_{\beta z}$ and $\bar{\sigma}_{zz}$ distributions through the thickness. The results demonstrated a good accuracy overall the thickness distributions with respect the LD4.

www.SID.ir

Archive of SID

Table 3. Dimensionless transverse displacement and stresses for 0°/90°/0° for $a/h=10$ shell under bi-sinusoidal loading.

R/a	Model	$\bar{w}$	Diff (%)	$\bar{\sigma}_{\alpha\alpha}$	Diff (%)	$\bar{\tau}_{\alpha z}$	Diff (%)	$\bar{\tau}_{\beta z}$	Diff (%)	$\bar{\sigma}_{zz}$	Diff (%)
5	LD4	7.3251	--	5.8298	--	3.4648	--	1.1908	--	0.2456	--
	ED4	6.9738	4.80	5.7676	1.07	3.5604	2.76	1.1480	3.59	0.2428	1.14
	HRM 12	7.3183	0.09	5.8174	0.21	3.4612	0.10	1.1932	0.20	0.2373	3.38
	HRM 15	7.3210	0.06	5.8198	0.17	3.4633	0.04	1.1931	0.19	0.237	3.50
	HRM 18	7.3220	0.04	5.8216	0.14	3.4647	0.00	1.1873	0.29	0.2346	4.48
	HRM 21	7.3238	0.02	5.8227	0.12	3.4656	0.02	1.1876	0.27	0.2446	0.41
10	LD4	7.5116	--	5.9345	--	3.5624	--	1.2245	--	0.3688	0.98
	ED4	7.1375	4.48	5.8699	1.09	3.6535	2.56	1.1782	3.78	0.3676	0.33
	HRM 12	7.5064	0.07	5.9329	0.03	3.5593	0.09	1.2271	0.21	0.3642	1.25
	HRM 15	7.5093	0.03	5.9354	0.02	3.5615	0.03	1.2270	0.20	0.364	1.30
	HRM 18	7.5103	0.02	5.9373	0.05	3.5630	0.02	1.2212	0.27	0.3627	1.65
	HRM 21	7.5108	0.01	5.9376	0.05	3.5632	0.02	1.2212	0.27	0.3682	0.16
20	LD4	7.5429	--	5.9424	--	3.5791	--	1.2303	--	0.4338	--
	ED4	7.1636	5.03	5.8703	1.24	3.6688	2.49	1.1832	3.80	0.4332	0.14
	HRM 12	7.5382	0.06	5.9362	0.13	3.5762	0.09	1.2330	0.24	0.4311	0.62
	HRM 15	7.5412	0.02	5.9388	0.09	3.5784	0.03	1.2329	0.24	0.4311	0.62
	HRM 18	7.5422	0.01	5.9406	0.06	3.5799	0.01	1.2270	0.24	0.4304	0.78
	HRM 21	7.5423	0.01	5.9408	0.05	3.5799	0.01	1.2270	0.24	0.4334	0.09
50	LD4	7.5407	--	5.9424	--	3.5782	--	1.2300	--	0.4732	--
	ED4	7.1605	5.04	5.8535	1.50	3.6674	2.49	1.1828	3.78	0.4729	0.06
	HRM 12	7.536	0.06	5.9199	0.38	3.5754	0.08	1.2327	0.28	0.4717	0.32
	HRM 15	7.539	0.02	5.9225	0.33	3.5776	0.02	1.2327	0.28	0.4717	0.32
	HRM 18	7.5400	0.01	5.9244	0.30	3.5791	0.03	1.2268	0.20	0.4714	0.38
	HRM 21	7.5401	0.01	5.9246	0.30	3.5791	0.03	1.2268	0.20	0.4729	0.06
100	LD4	7.5364	--	5.9163	--	3.5761	--	1.2293	--	0.4863	--
	ED4	7.1563	5.04	5.8451	1.64	3.6651	2.49	1.1821	3.84	0.4861	0.04
	HRM 12	7.5318	0.06	5.9114	0.52	3.5733	0.08	1.232	0.22	0.4853	0.21
	HRM 15	7.5348	0.02	5.914	0.48	3.5754	0.02	1.2319	0.21	0.4852	0.23
	HRM 18	7.5358	0.01	5.9159	0.45	3.5769	0.02	1.2261	0.26	0.485	0.27
	HRM 21	7.5358	0.01	5.9161	0.44	3.5769	0.02	1.2261	0.26	0.4861	0.04
1000	LD4	7.5310	--	5.9070	--	3.5734	--	1.2284	--	0.4981	--
	ED4	7.1512	5.04	5.8363	1.20	3.6623	2.49	1.1812	3.84	0.498	0.02
	HRM 12	7.5264	0.06	5.9025	0.08	3.5706	0.08	1.2311	0.22	0.4974	0.14
	HRM 15	7.5294	0.02	5.905	0.03	3.5727	0.02	1.231	0.21	0.4974	0.14
	HRM 18	7.5304	0.01	5.9069	0.00	3.5742	0.02	1.2252	0.26	0.4973	0.16
	HRM 21	7.5304	0.01	5.9072	0.00	3.5742	0.02	1.2252	0.26	0.4979	0.04

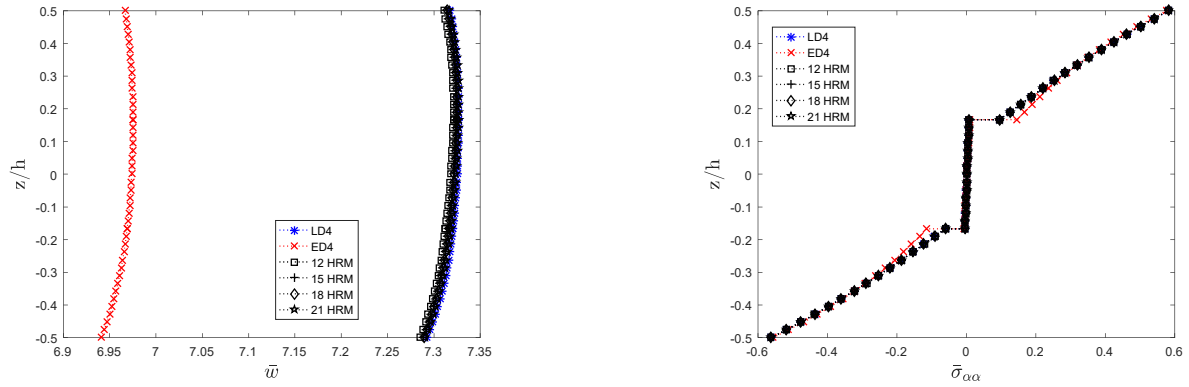

Fig. 4. Dimensionless displacement and stresses distribution for 0°/90°/0°, $a/h=10$, $R/a=5$ subjected to bi-sinusoidal loading.

www.SID.ir

Archive of SID

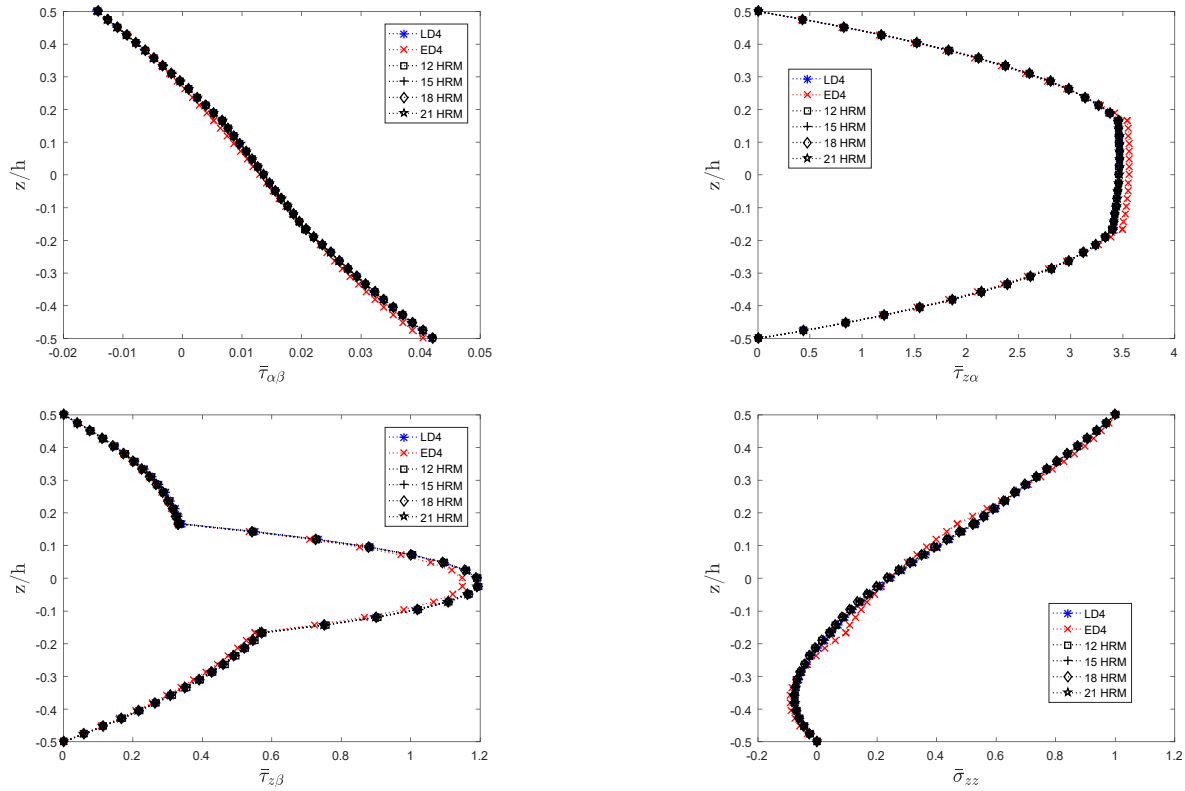

Fig. 4. Continued.

Figure 5 shows the relation between the dimensionless $\bar{w}$ and the inverse of curvature-radius-to-size (a/R) ratio for a moderate thick shell $a/h=10$. The displacements are compared with other HSDTs available in the literature such as the sinusoidal shear deformation theory proposed by Ferreira et al. [52], the third order shear deformation proposed by Reddy and Liu [12], optimized HSDT proposed by Mantari et al. [13], FSDT [12], a modified third order shear deformation theory proposed by Thakur et al. [50], the sinusoidal theory introduced by Touratier [53] and a higher order shear deformation theory which shear strain function combines exponential and trigonometric functions proposed by Mantari et al. [54]. This plot shows the interesting features of shells, i.e. it demonstrates that as the radius of curvature increase, the transverse displacement increase.

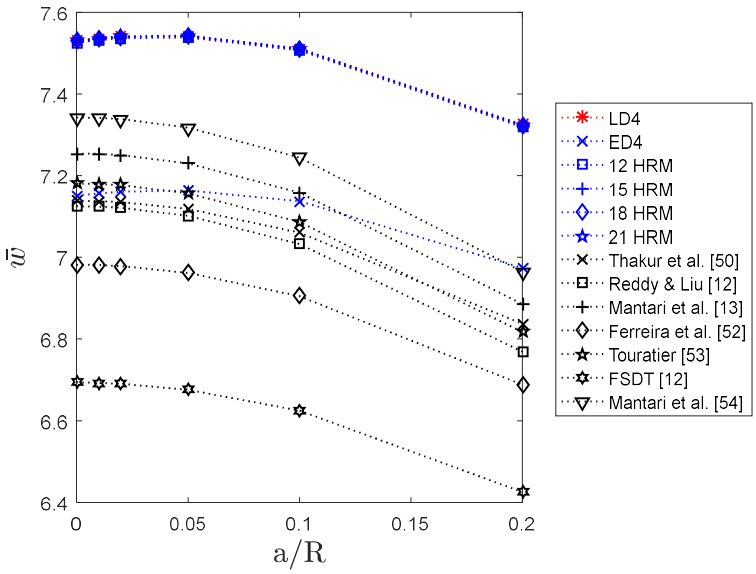

Fig. 5. Dimensionless transverse displacement $\bar{w}$ versus a/R ratio for 0°/90°/0°, $a/h=10$, subjected to bi-sinusoidal loading.

It is important to remark that the integrals of the solution of the 3D elasticity equations are easily to compute when the thickness functions are Maclaurin polynomial expansions, due to this integrals can be solved analytically. However, it is quite difficult to deal with refined models having non-polynomial expansions, due that integrals of the 3D elasticity solutions do not have an analytical solution. So the non-polynomial functions are transform into Taylor series in order to calculate some

www.SID.ir

Archive of SID

approximate integrals for solving the 3D elasticity equations for out-plane stresses.

Table 4. Dimensionless transverse displacement and stresses for 0°/90°/0° for a/h = 10 shell under uniform loading.

R/a	Model	$\bar{w}$	Diff(%)	$\bar{\sigma}_{\alpha\alpha}$	Diff(%)	$\bar{\tau}_{\alpha z}$	Diff(%)	$\bar{\tau}_{\beta z}$	Diff(%)	$\bar{\sigma}_{zz}$	Diff(%)
5	LD4	11.2067	--	8.5334	--	6.1181	--	3.9939	--	1.2427	--
	ED4	10.6606	4.87	8.441	1.11	6.2362	1.93	3.6507	8.59	1.2274	1.23
	HRM 12	11.2026	0.04	8.5205	0.17	6.0892	0.47	3.7282	6.65	1.1081	10.83
	HRM 15	11.2038	0.03	8.5202	0.18	6.1262	0.13	4.1762	4.56	1.1044	11.13
	HRM 18	11.2026	0.04	8.5207	0.17	6.0832	0.57	3.9139	2.00	0.8964	27.87
	HRM 21	11.2038	0.03	8.5225	0.15	6.0848	0.54	3.9114	2.07	1.1290	9.15
10	LD4	11.5076	--	8.7323	--	6.2707	--	4.0489	--	0.3064	--
	ED4	10.9248	5.06	8.6253	1.23	6.3817	-2.51	3.7023	8.56	0.3063	0.03
	HRM 12	11.5062	0.01	8.7258	0.07	6.2428	0.14	3.7870	6.47	0.2976	2.87
	HRM 15	11.5078	0.00	8.7258	0.07	6.2798	0.08	4.2302	4.48	0.2974	2.94
	HRM 18	11.5068	0.01	8.7263	0.07	6.2373	0.03	3.9700	1.95	0.2786	9.07
	HRM 21	11.5076	0.00	8.7270	0.06	6.2378	0.03	3.9671	2.02	0.2956	3.52
20	LD4	11.5595	--	8.7462	--	6.2952	--	4.0537	--	0.4027	--
	ED4	10.9683	5.11	8.6372	1.25	6.4040	1.73	3.707	8.55	0.4033	0.15
	HRM 12	11.5589	0.01	8.7426	0.04	6.2678	0.44	3.7936	6.42	0.3966	1.51
	HRM 15	11.5604	0.01	8.7426	0.04	6.3046	0.15	4.2343	4.46	0.3965	1.54
	HRM 18	11.5595	0.00	8.7432	0.03	6.2624	0.52	3.9754	1.93	0.3788	5.93
	HRM 21	11.5598	0.00	8.7436	0.03	6.2626	0.52	3.9754	1.93	0.3925	2.53
50	LD4	11.5571	--	8.7259	--	6.2924	--	4.0489	--	0.4612	--
	ED4	10.9645	5.13	8.6175	1.24	6.4004	1.72	3.7027	8.55	0.4620	0.17
	HRM 12	11.5567	0.00	8.7237	0.03	6.2651	0.43	3.7899	6.40	0.4567	0.98
	HRM 15	11.5583	0.01	8.7237	0.03	6.3018	0.15	4.229	4.45	0.4567	0.98
	HRM 18	11.5574	0.00	8.7244	0.02	6.2598	0.52	3.9709	1.93	0.4396	4.68
	HRM 21	11.5574	0.00	8.7248	0.01	6.2599	0.52	3.9679	2.00	0.4512	2.17
100	LD4	11.5507	--	8.7143	--	6.2885	--	4.0460	--	0.4807	--
	ED4	10.9581	5.13	8.6064	1.24	6.3963	1.71	3.7000	8.55	0.4816	0.19
	HRM 12	11.5502	0.00	8.7126	0.02	6.2612	0.43	3.7873	6.39	0.4768	0.81
	HRM 15	11.5518	0.01	8.7126	0.02	6.2979	0.15	4.2260	4.45	0.4767	0.83
	HRM 18	11.5509	0.00	8.7132	0.01	6.2559	0.52	3.9682	1.92	0.4598	4.35
	HRM 21	11.551	0.00	8.7137	0.01	6.256	0.52	3.9651	2.00	0.4708	2.06
1000	LD4	11.5424	--	8.7018	--	6.2837	--	4.0429	--	0.4981	--
	ED4	10.9503	5.13	8.5946	1.23	6.3914	1.71	3.6972	8.55	0.4992	0.22
	HRM 12	11.542	0.00	8.7005	0.01	6.2564	0.43	3.7845	6.39	0.4948	0.66
	HRM 15	11.5436	0.01	8.7005	0.01	6.2931	0.15	4.2227	4.45	0.4948	0.66
	HRM 18	11.5427	0.00	8.7012	0.01	6.2512	0.52	3.9652	1.92	0.4781	4.02
	HRM 21	11.5428	0.00	8.7016	0.00	6.2513	0.52	3.962	2.00	0.4884	1.95

5.1.2. Distributed uniform loading

Doubly-curved panel subjected to distribute uniform loading are investigated (see Figure 2). In order to approximate the load, an approximation of Navier series with $m = n = 90$ in Equation 34 (see Ref. [12, 37]).

The results for moderate thick panels ($a/h = 10$) are presented in Table 4. It is denoted that for transverse displacement $\bar{w}$, the error of ED4 is a maximum of 5.13% while HRM presented a maximum error of 0.04%. In term of normal stress $\bar{\sigma}_{\alpha\alpha}$ excellent agreements are obtained using the HRM with a maximum error of 0.18%. The results demonstrate that the HRM with 18 variables is the best model for evaluating the transverse shear stress $\bar{\tau}_{\beta z}$. ED4 is the best models for predicting the normal stress $\bar{\sigma}_{zz}$.

www.SID.ir

Archive of SID

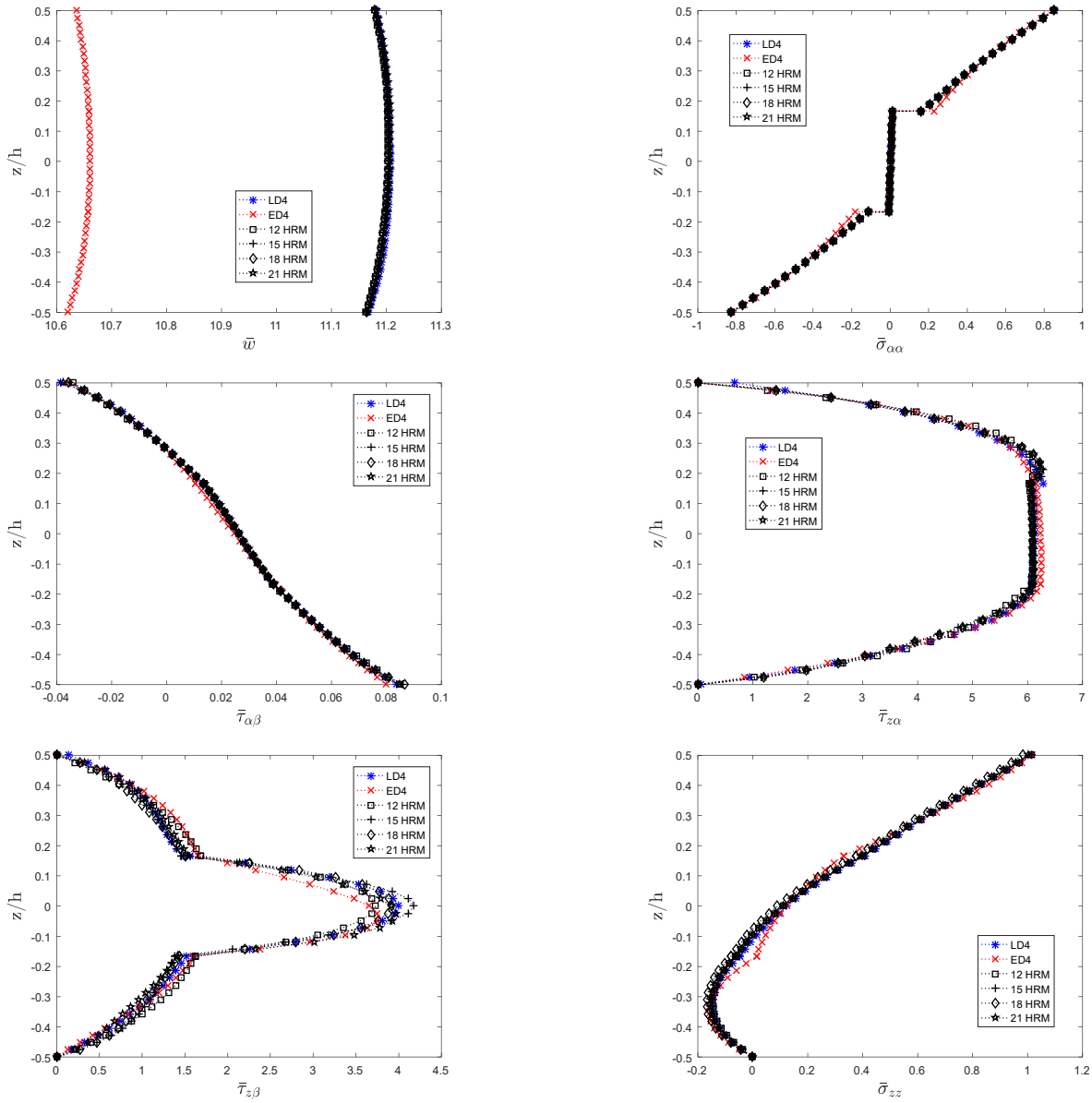

Fig. 6. Dimensionless transverse displacement and stresses distribution for 0°/90°/0°, $a/h=10$, $R/a=5$ subjected to uniform distributed loading.

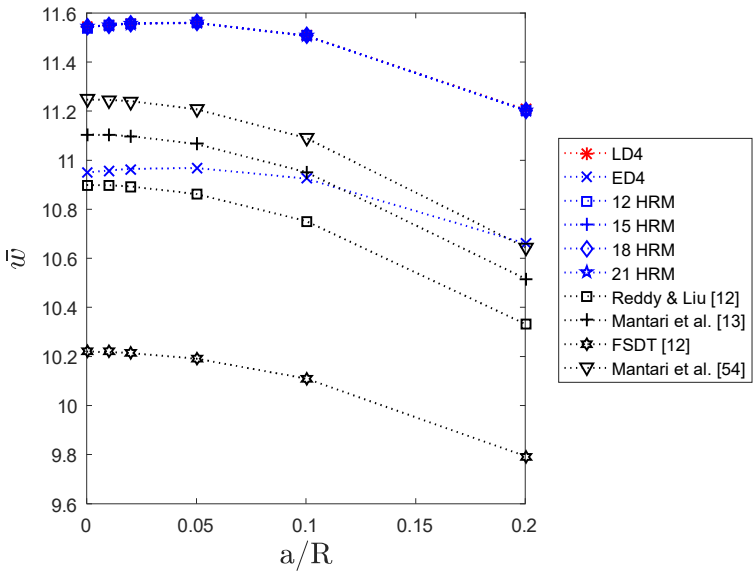

Fig. 7. Dimensionless transverse displacement $\bar{w}$ versus a/R ratio for 0°/90°/0°, $a/h = 10$, subjected to uniform distributed loading.

www.SID.ir

Archive of SID

The calculated error for the transverse displacement of the HRM increase as the ratio *a/R* decreases. Figure 6 shows the distribution of dimensionless displacement $\bar{w}$ and stresses $\bar{\sigma}_{\alpha\alpha}, \bar{\tau}_{\alpha\beta}, \bar{\tau}_{\alpha z}, \bar{\tau}_{\beta z}$ and $\bar{\sigma}_{zz}$. Overall, good agreements are obtained for the stresses and displacements through the thickness distribution. Furthermore, it is demonstrated that 18 HRM and 21 HRM can predict better the through the thickness distribution of $\bar{\tau}_{\beta z}$.

Figure 7 shows the dimensionless transverse displacement versus *a/R* ratio. The results of HSDTs of Reddy and Liu [12], Mantari et al. [13, 54] and FSDT [12] are included. The results of normalized transverse displacement of the presented displacement fields are higher than LD4. It is demonstrated that as *a/R* ratio increases, the transverse displacement decreases.

5.1.3. Patch loading

Moderate thick doubly-curved (*a/h* = 10) panel subjected to uniform patch loading are investigated (see Figure 2). The area of the patch is described as the following: $(a/4 \le \alpha \le 3a/4, b/4 \le \beta \le 3b/4)$. Figure 8 shows the convergence of transverse displacement $\bar{w}$ and transverse shear stress $\bar{\tau}_{\alpha z}$ for *a/R* = 5. It is determined that to calculate stresses with four decimal precision, the Navier series parameters "*m*" and "*n*" are set equal to 90 (see Equation (29)). However for transverse displacements this parameters of the Navier series can be set as 30.

Different results for stresses and displacements are presented in Table 5 considering a thickness ratio of $a/h = 10$. In all the case of transverse displacement, the maximum error is around 4.98%, while HRM presented a maximum error of 0.14% considering the different *R/a* ratios. Good agreements are obtained for stresses $\bar{\sigma}_{\alpha\alpha}$ and $\bar{\tau}_{\alpha z}$ since they have a maximum error of 0.52% and 0.25%, respectively. Results demonstrated that HRMs with 18 and 21 variables predict better the transverse shear stress $\bar{\tau}_{\beta z}$ with a maximum error of 0.12% overall *a/R* ratios. For this particular stress there are certain discrepancy respect using the HRMs with 12 and 15 variables, however the percentages error of this model are less than ED4. The results demonstrate that for $\bar{\tau}_{\beta z}$, the error increases as the *R/a* ratio decreases. It is demonstrated that for the transverse normal stress $\bar{\sigma}_{zz}$, the best model strictly depends on the curvature-radius-to-size ratio.

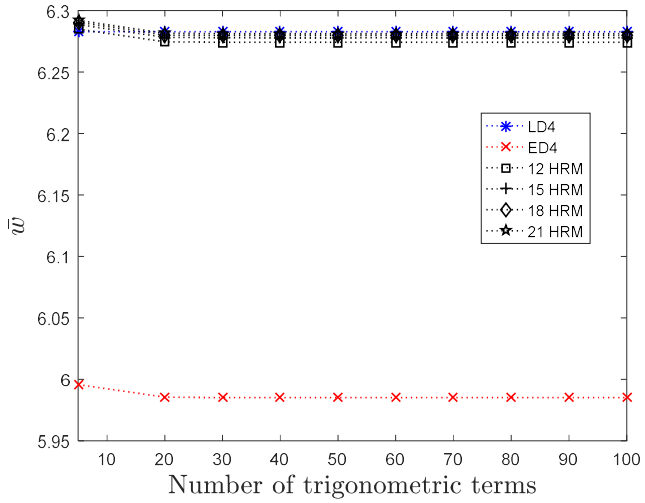

(a)

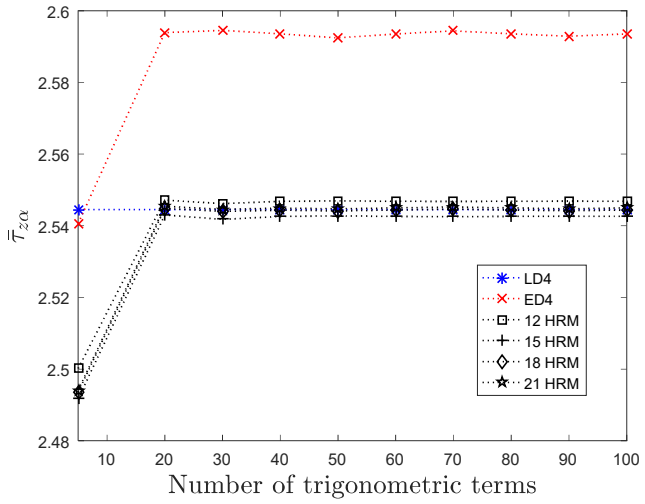

(b)

Fig. 8. Convergence of solution of transverse displacement $\bar{w}$ and transverse shear stress $\bar{\tau}_{\alpha z}$ for patch loading.

www.SID.ir

Archive of SID

Table 5. Dimensionless transverse displacement and stresses for 0°/90°/0° for $a/h=10$ shell under uniform patch loading.

R/a	Model	$\bar{w}$	Diff(%)	$10\times\bar{\sigma}_{\alpha\alpha}$	Diff(%)	$10^2\times\bar{\tau}_{\alpha z}$	Diff(%)	$10^2\times\bar{\tau}_{\beta z}$	Diff(%)	$\bar{\sigma}_{zz}$	Diff(%)
5	LD4	6.2829	--	5.1865	--	2.5445	--	0.1619	--	0.2763	--
	ED4	5.9852	4.74	5.1328	1.37	2.5929	1.71	0.1146	29.22	0.2736	0.83
	HRM 12	6.2742	0.14	5.1780	0.50	2.5469	0.09	0.1426	11.92	0.2688	2.57
	HRM 15	6.2778	0.08	5.1769	0.52	2.5427	0.25	0.1560	3.64	0.2686	2.65
	HRM 18	6.2797	0.05	5.1796	0.47	2.5442	0.20	0.1620	0.06	0.2658	3.66
	HRM 21	6.2812	0.03	5.1805	0.45	2.5447	0.18	0.1621	0.12	0.2768	0.33
10	LD4	6.4346	--	5.2693	--	2.6265	--	0.1877	--	0.3860	--
	ED4	6.1183	4.96	5.2077	1.17	2.6716	1.72	0.1378	26.58	0.3850	0.26
	HRM 12	6.4273	0.11	5.2646	0.09	2.6292	0.10	0.1687	10.12	0.3822	0.98
	HRM 15	6.4310	0.05	5.2636	0.11	2.6251	0.05	0.1820	3.04	0.3821	1.01
	HRM 18	6.4329	0.02	5.2664	0.06	2.6267	0.01	0.1879	0.11	0.3803	1.48
	HRM 21	6.4334	0.02	5.2666	0.05	2.6268	0.01	0.1878	0.05	0.3869	0.23
20	LD4	6.4593	--	5.2656	--	2.6413	--	0.1939	--	0.4437	--
	ED4	6.1389	4.96	5.2033	1.18	2.6854	1.67	0.1434	26.04	0.4434	0.07
	HRM 12	6.4524	0.11	5.2626	0.06	2.6441	0.11	0.1749	9.80	0.4418	0.43
	HRM 15	6.4562	0.05	5.2616	0.08	2.6401	0.05	0.1882	2.94	0.4417	0.45
	HRM 18	6.4581	0.02	5.2645	0.02	2.6416	0.01	0.1940	0.05	0.4405	0.72
	HRM 21	6.4582	0.02	5.2646	0.02	2.6417	0.02	0.1939	0.00	0.4448	0.25
50	LD4	6.4569	--	5.2483	--	2.6413	--	0.1952	--	0.4786	--
	ED4	6.1357	4.97	5.1866	1.18	2.6851	1.66	0.1447	25.87	0.4787	0.02
	HRM 12	6.4500	0.11	5.2463	0.04	2.6442	0.11	0.1764	9.63	0.4778	0.17
	HRM 15	6.4538	0.05	5.2453	0.06	2.6401	0.05	0.1896	2.87	0.4778	0.17
	HRM 18	6.4558	0.02	5.2481	0.00	2.6417	0.02	0.1954	0.10	0.4770	0.33
	HRM 21	6.4558	0.02	5.2482	0.00	2.6417	0.02	0.1953	0.05	0.4798	0.25
100	LD4	6.4531	--	5.2401	--	2.6399	--	0.1953	--	0.4902	--
	ED4	6.1320	4.98	5.1786	1.17	2.6835	1.65	0.1447	25.91	0.4905	0.06
	HRM 12	6.4463	0.11	5.2383	0.03	2.6427	0.11	0.1765	9.63	0.4898	0.08
	HRM 15	6.4501	0.05	5.2373	0.05	2.6386	0.05	0.1897	2.87	0.4898	0.08
	HRM 18	6.4520	0.02	5.2401	0.00	2.6402	0.01	0.1955	0.10	0.4891	0.22
	HRM 21	6.4521	0.02	5.2402	0.00	2.6402	0.01	0.1954	0.05	0.4915	0.27
1000	LD4	6.4485	--	5.2315	--	2.6379	--	0.1952	--	0.5007	--
	ED4	6.1276	4.98	5.1705	1.17	2.6815	1.65	0.1447	25.87	0.5011	0.08
	HRM 12	6.4417	0.11	5.2300	0.03	2.6407	0.11	0.1764	9.63	0.5007	0.00
	HRM 15	6.4455	0.05	5.2290	0.05	2.6367	0.05	0.1896	2.87	0.5007	0.00
	HRM 18	6.4474	0.02	5.2318	0.01	2.6382	0.01	0.1954	0.10	0.5000	0.14
	HRM 21	6.4474	0.02	5.2320	0.01	2.6382	0.01	0.1953	0.05	0.5020	0.26

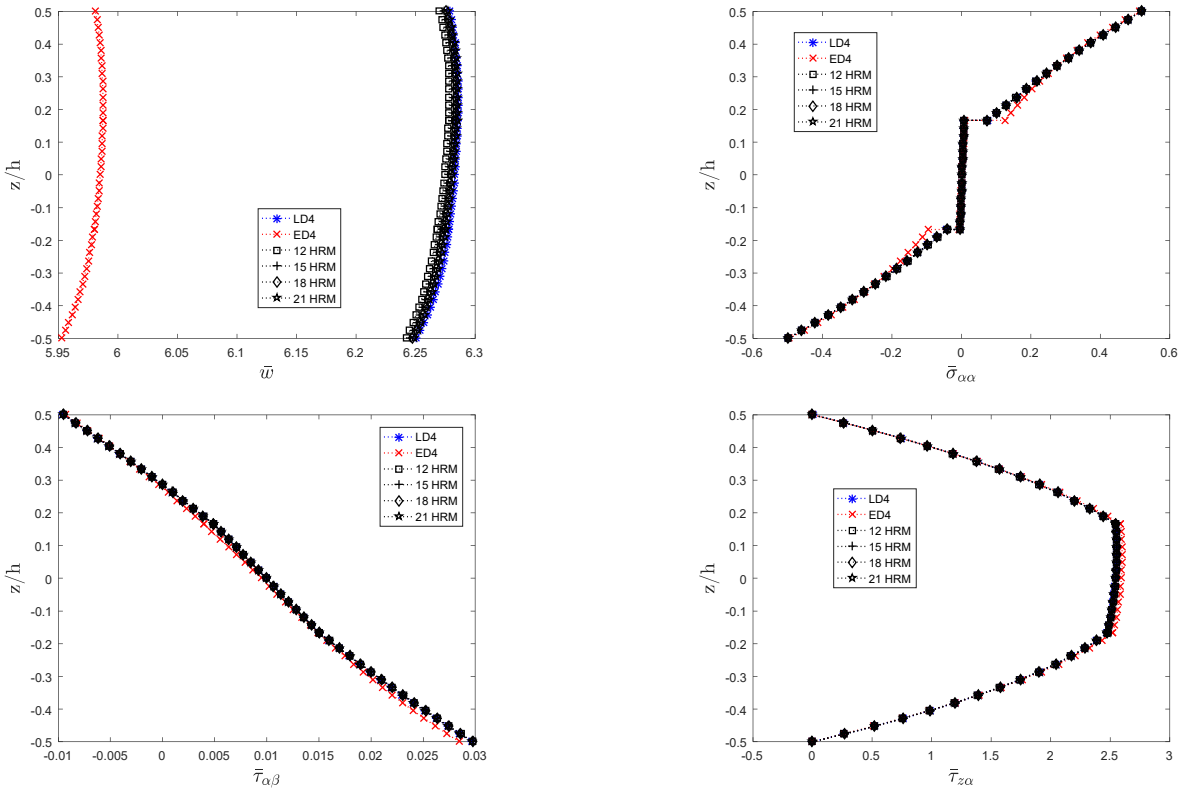

Fig. 9. Dimensionless transverse displacement and stresses through the thickness distribution for 0°/90°/0°, $a/h=10$, $R/a=5$ subjected to uniform patch loading.

www.SID.ir

Archive of SID

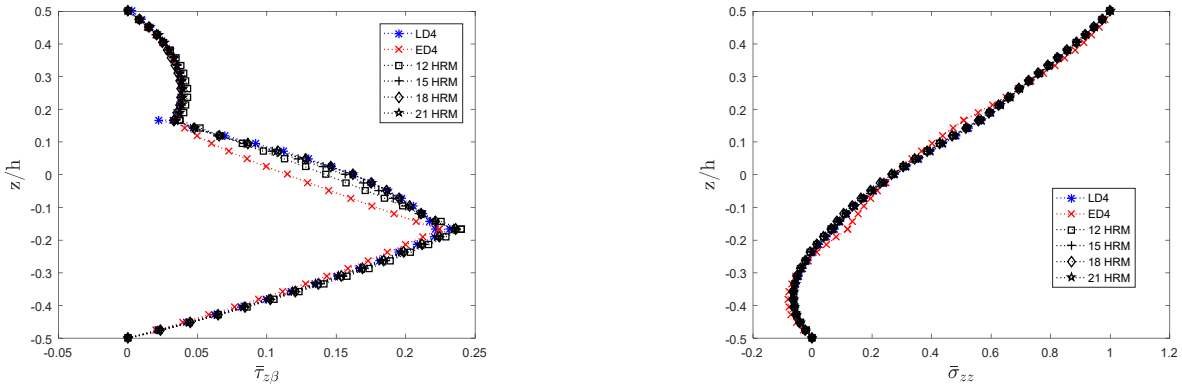

Fig. 9. Continued.

Figure 9 shows the distribution of displacement $\bar{w}$ and stresses $\bar{\sigma}_{\alpha\alpha}, \bar{\tau}_{\alpha\beta}, \bar{\tau}_{\alpha z}, \bar{\tau}_{\beta z}$ and $\bar{\sigma}_{zz}$. The thought the thickness distribution show a certain discrepancy of the stress $\bar{\tau}_{\beta z}$ for ED4 model and HRM with 12 and 15 variables.

5.1.4. Hydrostatic loading

Moderately thick shell $(a/h=10)$ subjected to a hydrostatic loading is investigated (see Figure 2). The convergence for dimensionless transverse displacements and transverse shear stress $\bar{\tau}_{\alpha z}$ is shown in Figure 10. The trigonometrical terms are set as $m=n=90$ for the Navier trigonometrical series. It is demonstrated that HRM with 12 and 15 variables converges faster than HRM with 18 and 21 variables. Table 6 report the transverse displacement $\bar{w}$ and stresses $\bar{\sigma}_{\alpha\alpha}, \bar{\tau}_{\alpha z}, \bar{\tau}_{\beta z}$ and $\bar{\sigma}_{zz}$. The results for transverse displacement are the same for all the HRMs presented with a maximum error of 0.04% while ED4 present a maximum of 5.13%. The error of transverse displacement increases as the a/R ratio decreases. Good agreements are obtained for transverse shear stress $\bar{\tau}_{\alpha z}$ with a maximum error of 0.57%. The best model in predicting $\bar{\tau}_{\alpha z}$ is the HRM with 12 variables. It is demonstrated that HRM models with 18 and 21 variables can predict better the transverse shear stress $\bar{\tau}_{\beta z}$ with a maximum of 2.0% and 2.07%, respectively overall the R/a ratios. The best results for transverse normal stresses are captured by ED4.

Table 6. Dimensionless transverse displacement and stresses for 0°/90°/0° for $a/h=10$ shell under hydrostatic loading.

R/a	Model	$\bar{w}$	Diff(%)	$10\times\bar{\sigma}_{\alpha\alpha}$	Diff(%)	$10^2\times\bar{\tau}_{\alpha z}$	Diff(%)	$10^2\times\bar{\tau}_{\beta z}$	Diff(%)	$\bar{\sigma}_{zz}$	Diff(%)
5	LD4	5.6033	--	4.2667	--	3.0590	--	1.9970	--	0.0623	--
	ED4	5.3303	4.87	4.2205	1.08	3.1181	1.93	1.8254	8.59	0.0614	1.44
	HRM 12	5.6013	0.04	4.2602	0.15	3.0446	0.47	1.8641	6.65	0.0554	11.08
	HRM 15	5.6019	0.02	4.2601	0.15	3.0631	0.13	2.0881	4.56	0.0552	11.40
	HRM 18	5.6014	0.03	4.2603	0.15	3.0416	0.57	1.957	2.00	0.0448	28.09
	HRM 21	5.6029	0.01	4.2612	0.13	3.0424	0.54	1.9557	2.07	0.0565	9.31
10	LD4	5.7538	--	4.3661	--	3.1353	--	2.0244	--	0.1532	--
	ED4	5.4624	5.06	4.3126	1.23	3.1908	1.77	1.8512	8.56	0.1532	0.00
	HRM 12	5.7531	0.01	4.3629	0.07	3.1214	0.44	1.8935	6.47	0.1488	2.87
	HRM 15	5.7539	0.00	4.3629	0.07	3.1399	0.15	2.1151	4.48	0.1487	2.94
	HRM 18	5.7534	0.01	4.3632	0.07	3.1187	0.53	1.985	1.95	0.1393	9.07
	HRM 21	5.7538	0.00	4.3635	0.06	3.1189	0.52	1.9835	2.02	0.1478	3.52
20	LD4	5.7798	--	4.3731	--	3.1476	--	2.0268	--	0.2014	--
	ED4	5.4842	5.11	4.3186	1.25	3.202	1.73	1.8535	8.55	0.2016	0.10
	HRM 12	5.7794	0.01	4.3713	0.04	3.1339	0.44	1.8968	6.41	0.1983	1.54
	HRM 15	5.7802	0.01	4.3713	0.04	3.1523	0.15	2.1171	4.46	0.1983	1.54
	HRM 18	5.7798	0.00	4.3716	0.03	3.1312	0.52	1.9877	1.93	0.1894	5.96
	HRM 21	5.7799	0.00	4.3718	0.03	3.1313	0.52	1.9862	2.00	0.1962	2.58
50	LD4	5.7786	--	4.3629	--	3.1462	--	2.0244	--	0.2306	--
	ED4	4.4842	22.40	4.3088	1.24	3.2002	1.72	1.8513	8.55	0.231	0.17
	HRM 12	5.7783	0.01	4.3619	0.02	3.1325	0.44	1.8949	6.40	0.2284	0.95
	HRM 15	5.7791	0.00	4.3619	0.02	3.1509	0.15	2.1145	4.45	0.2283	1.00

www.SID.ir

Archive of SID

Table 6. Continued

R / a	Model	$\bar{w}$	Diff(%)	$10\times\bar{\sigma}_{\alpha\alpha}$	Diff(%)	$10^2\times\bar{\tau}_{\alpha z}$	Diff(%)	$10^2\times\bar{\tau}_{\beta z}$	Diff(%)	$\bar{\sigma}_{zz}$	Diff(%)
50	HRM 18	5.7787	0.00	4.3622	0.02	3.1299	0.52	1.9855	1.92	0.2198	4.68
	HRM 21	5.7787	0.00	4.3624	0.01	3.1299	0.52	1.9839	2.00	0.2256	2.17
100	LD4	5.7753	--	4.3571	--	3.1443	--	2.0230	--	0.2403	--
	ED4	5.4791	5.13	4.3032	1.24	3.1982	1.71	1.8500	8.55	0.2408	0.21
	HRM 12	5.7751	0.00	4.3563	0.02	3.1306	0.44	1.8937	6.39	0.2384	0.79
	HRM 15	5.7759	0.01	4.3563	0.02	3.1489	0.15	2.1130	4.45	0.2384	0.79
	HRM 18	5.7755	0.00	4.3566	0.01	3.1280	0.52	1.9841	1.92	0.2299	4.33
	HRM 21	5.7755	0.00	4.3568	0.01	3.1280	0.52	1.9825	2.00	0.2354	2.04
1000	LD4	5.7712	--	4.3509	--	3.1419	--	2.0214	--	0.2491	--
	ED4	5.4751	5.13	4.2973	1.23	3.1957	1.71	1.8486	8.55	0.2496	0.20
	HRM 12	5.7710	0.00	4.3502	0.02	3.1282	0.44	1.8923	6.39	0.2474	0.68
	HRM 15	5.7718	0.01	4.3503	0.01	3.1465	0.15	2.1114	4.45	0.2474	0.68
	HRM 18	5.7714	0.00	4.3506	0.01	3.1256	0.52	1.9826	1.92	0.2390	4.05
	HRM 21	5.7714	0.00	4.3508	0.00	3.1256	0.52	1.9810	2.00	0.2442	1.97

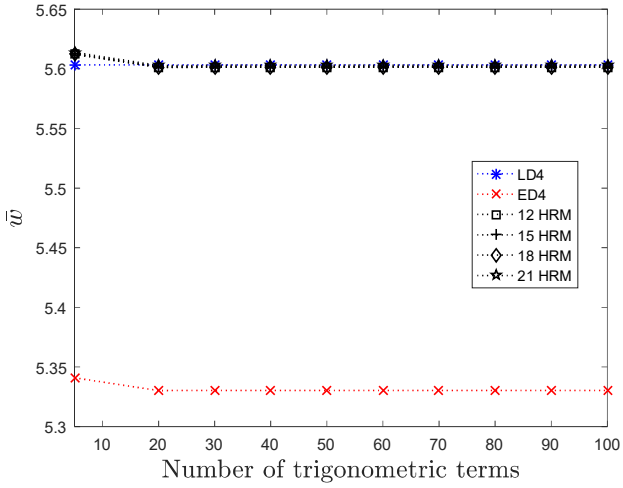

(a)

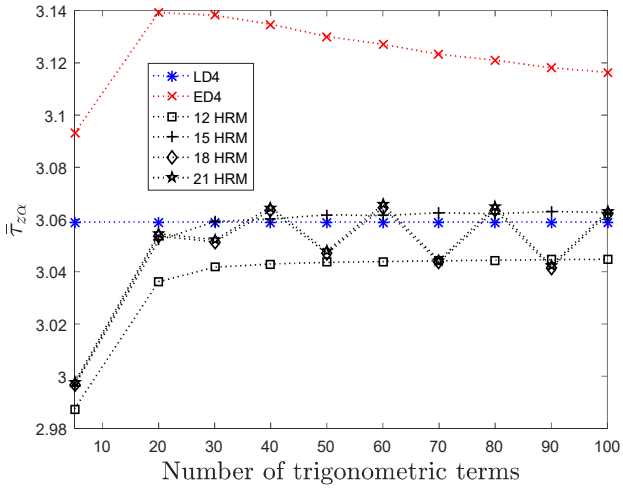

(b)

Fig. 10. Convergence of solution of transverse displacement $\bar{w}$ and transverse shear stress $\bar{\tau}_{\alpha z}$ for hydrostatic pressure.

Figure 11 shows the normalized stresses and transverse displacement for $R/a = 5$. HRM present a similar response to the static behavior predicted using LD4. It is demonstrated that the transverse displacement is higher for plate.

www.SID.ir

Archive of SID

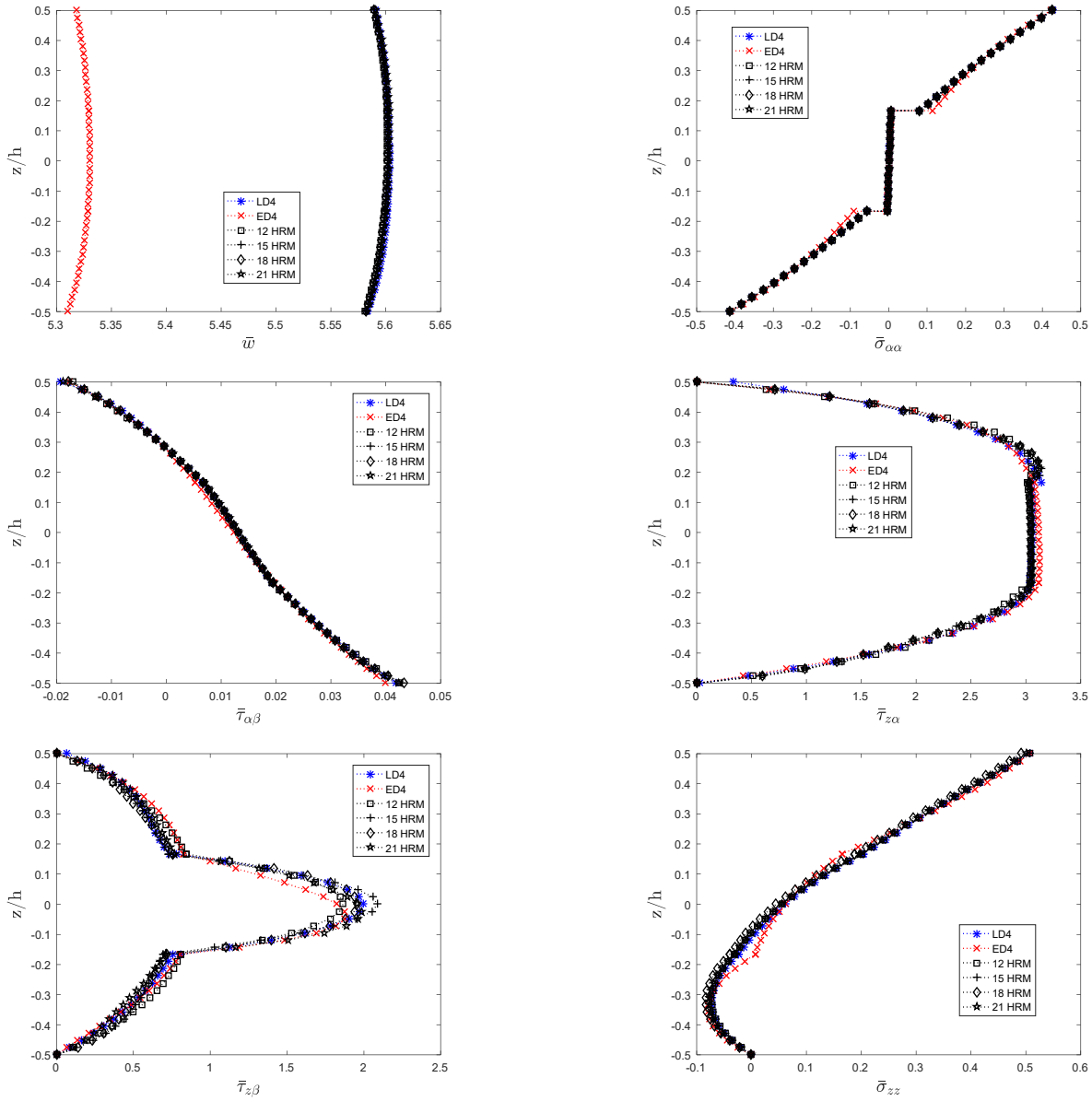

Fig. 11. Dimensionless displacement and stresses through the thickness distribution for 0°/90°/0°, $a/h=10$, $R/a=5$ subjected to hydrostatic loading.

5.1.5. Point loading

Moderate thick panel (*a/h = 10*) subjected to centered point loading (see Figure 2). The *m* and *n* parameters of Equation (29) are equal to 120, see previous works by Giunta et al. [37], Mantari et al. [13] and Reddy and Liu [12]. For this example, the following non-dimensional form of displacement is adopted:

$$\bar{w}=\frac{10^2 E_2 h^3 u_z}{P_z a^4} \tag{41}$$

The numerical results of displacements are presented in Table 7. The results are compared with HSDT by Mantari et al. [13], Reddy and Liu [12] and FSDT [12]. The results demonstrate that the higher numerical values overall the *a*/*R* ratio are reported by the FSDT. Figure 12 shows the relation between non-dimensional transverse displacement and *a*/*R* ratio. It can be seen, that the deflection decreases as the ratio *a*/*R* increases. The distribution of transverse displacement $\bar{w}$, normal stress $(\bar{\sigma}_{\alpha\alpha})$, transverse in-plane stress $(\bar{\tau}_{\alpha\beta})$, transverse shear stress $(\bar{\tau}_{\alpha z}, \bar{\tau}_{\beta z})$ and transverse normal stress $(\bar{\sigma}_{zz})$ for $R/a=5$ is shown in Figure 12.

It is noted that the transverse displacement calculated with HRM presents certain discrepancy with respect to LD4. The graphs demonstrated that ED4 present a better static behavior for transverse displacement. As it is described in the paper of Giunta et al. [37] point load induced high gradients in the displacement fields on the shell's top. And this may be the reason why polynomials functions predict better the static behavior of shells under point load. All the solutions proposed in this paper, satisfy the zero shear stress for the transverse normal stress, however, the HRM with 18 variables cannot reproduce the

www.SID.ir

Archive of SID

thought-the-thickness behavior for this particular stress. The LD4 solution presented discrepancy and inaccuracy in the shell's top for normal stresses. The LD4 solution do not meet the condition of zero shear stress at the top of the shell for $\overline{\tau}_{\alpha z}$ and $\overline{\tau}_{\beta z}$, so a refinement using a stress recovery procedure using 3D elasticity equations could be used. However, this problem can be improved by adding more mathematical layers at the shell's top [37].

Table 7. Dimensionless transverse displacement for 0°/90°/0° for a/h = 10 shell under centered point loading.

R/a	5	10	20	50	100	Plate
Reddy and Liu [12]	4.4340	4.5470	4.5765	4.5848	4.5861	4.5865
Mantari [13]	4.3665	4.4831	4.5137	4.5224	4.5236	4.5240
FSDT [12]	5.1410	5.2273	5.2594	5.2657	5.2666	5.2572
Mantari [54]	4.2993	4.4184	4.4497	4.4585	4.4598	4.4602
LD4	4.6492	4.7144	4.7206	4.7154	4.7081	4.7081
ED4	4.6275	4.6831	4.6871	4.6815	4.6782	4.6743
12 HRM	4.7895	4.8537	4.8593	4.8536	4.8502	4.8460
15 HRM	4.8139	4.8781	4.8835	4.8778	4.8744	4.8702
18 HRM	4.6202	4.6863	4.6927	4.6875	4.6842	4.6802
21 HRM	4.6326	4.6983	4.7046	4.6994	4.6961	4.6921

It is remarked that Point load verify the *case dependent problem* due to the strong discontinuity that has to be inserted in the structural model [51]. Future works will be focused on obtaining accuracy theories for the evaluation of stresses of plates subjected to point and line load.

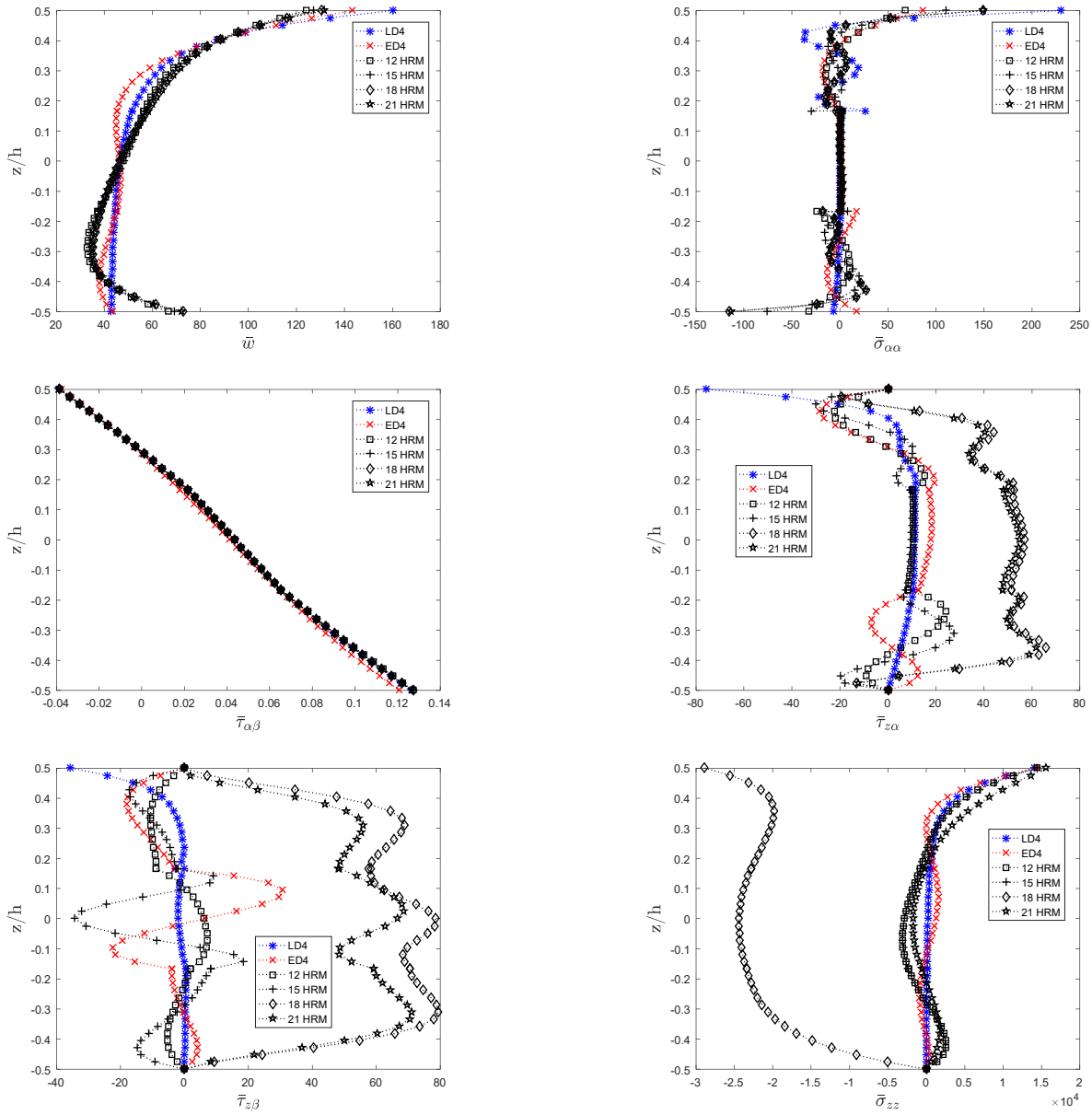

Fig. 12. Dimensionless transverse displacement $\overline{w}$ and stresses through the thickness distribution for 0°/90°/0°, $a/h = 10$, $R/a = 5$ subjected to centered point loading.

www.SID.ir

Archive of SID

5.2. Case 2

The present case problem was studied by Demasi [18] for plate configuration. In this paper, it is extended to doubly-curvature panel. The problem consists in a shell made by two different laminas subjected to bi-sinusoidal loading. The mechanical properties of layers are: $E_1 = 25E_2, E_1 = 25E_3, E_1 = 50G_{12}, E_1 = 50G_{13}, E_1 = 125G_{23}, \theta = 0°$ for the bottom and $E_1 = 25E_2, E_1 = 2.5E_3, E_1 = 50G_{12}, E_1 = 50G_{13}, E_1 = 125G_{23}, \theta = 90°$ for the top. The Poisson ratio is considered as: $\nu_{12} = \nu_{13} = \nu_{23} = 0.25$ for both layers. The thickness ratio is considered as $a/h = 4$. Different curvature-radius-to-size ratios are investigated. The next dimensionless form of transverse displacement and stresses are adopted:

$$\bar{w} = \frac{100h^3 E_2^{k=1} u_z}{P_z a^4}, \bar{\sigma}_{\alpha\alpha} = \frac{h^2}{a^2 P_z}\sigma_{\alpha\alpha}, (\bar{\tau}_{\alpha z}, \bar{\tau}_{\beta z}) = \frac{h}{aP_z}(\tau_{\alpha z}, \tau_{\beta z}) \tag{42}$$

The transverse displacement u_z is evaluated in $(a/2, b/2, 0)$, $\bar{\sigma}_{\alpha\alpha}, \bar{\tau}_{\alpha z}$ and $\bar{\tau}_{\beta z}$ is calculated at $(a/2, b/2, h/4)$, $(0, b/2, h/4)$ and $(a/2, 0, h/4)$, respectively.

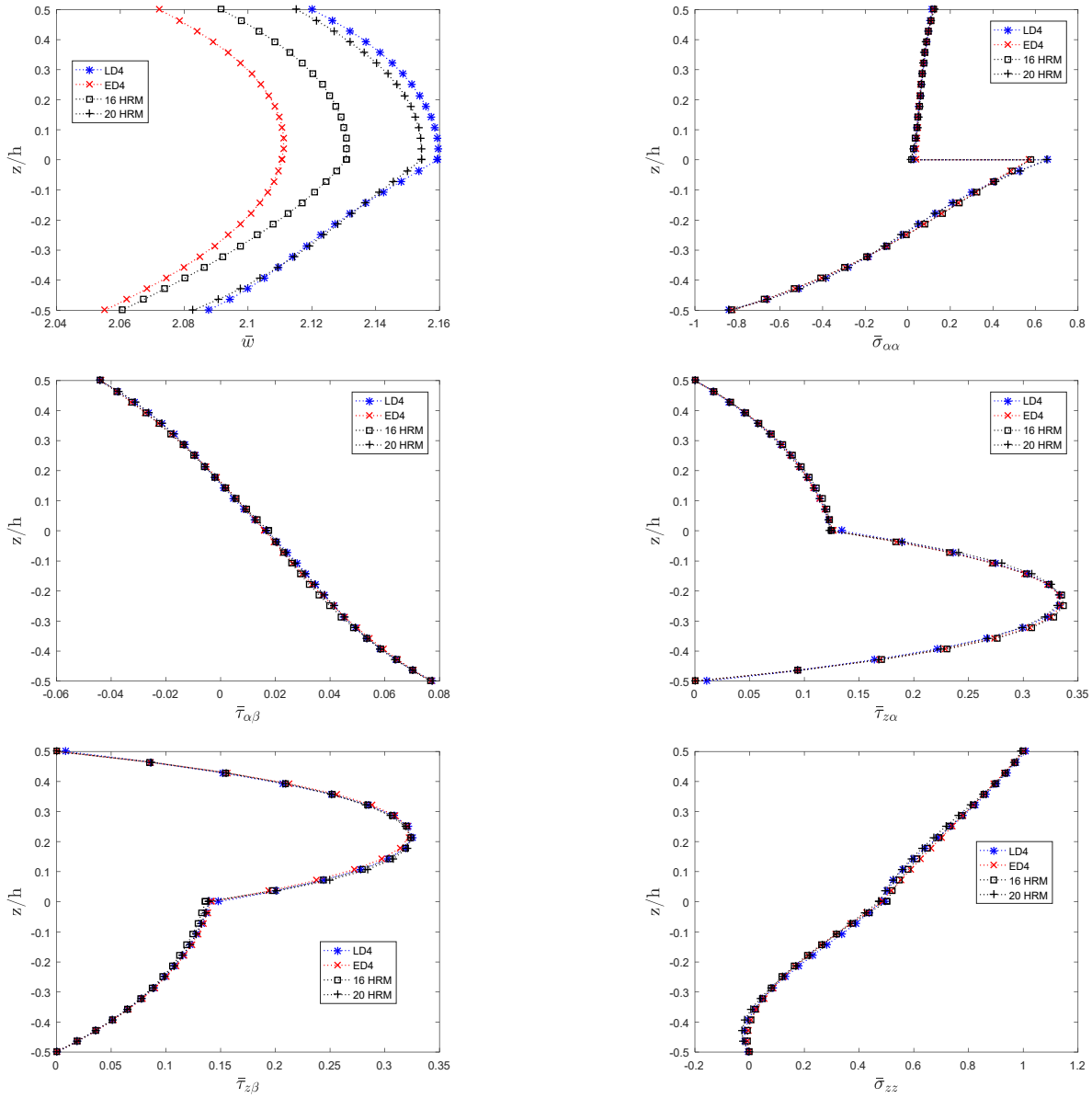

Fig. 13. Distribution of dimensionless transverse and stresses for Demasi's benchmark.

The HRM used for this example are: 16 HRM and 20 HRM (see Table 1). The following refined models were obtained with a similar methodology of previous work by Yarasca et al. [30]. It is demonstrated that for this case, the influence of trigonometrical, exponential and zig-zag combinations should be considered for obtaining good agreements. The presented results are compared with layerwise approach. Figure 13 presented the through thickness distributions for deep shells $(R/a = 5)$ for the transverse displacement $\bar{u}_z$ and the stresses $\bar{\sigma}_{\alpha\alpha}, \bar{\tau}_{\alpha\beta}, \bar{\tau}_{\alpha z}, \bar{\tau}_{\beta z}$ and $\bar{\sigma}_{zz}$. Good agreements are obtained overall the thickness distribution. The numerical results of transverse displacements and stresses are presented in Table 8. The results

www.SID.ir

Archive of SID

demonstrate that ED4 presented a better accuracy for $\bar{\tau}_{\beta z}$ with a maximum error of 0.58% while HRM with 20 variables presented 0.80% overall R/a ratios. The error of ED4 for transverse displacement decreases as the a/R ratio decreases. The best model in predicting the normal stress $\bar{\sigma}_{\alpha\alpha}$ is the HRM with 16 variables.

Table 8. Dimensionless stresses and transverse displacement for Demasi's Benchmark.

R/a	Model	$\bar{w}$	Diff(%)	$\bar{\sigma}_{\alpha\alpha}$	Diff(%)	$\bar{\tau}_{\alpha z}$	Diff(%)	$\bar{\tau}_{\beta z}$	Diff(%)
5	LD4	2.1594	--	6.3597	--	8.7875	--	3.2172	--
	ED4	2.1106	2.26	6.0764	4.45	8.7901	0.03	3.2042	0.40
	16 HRM	2.1307	1.33	6.2833	1.20	8.6421	1.65	3.1955	0.67
	20 HRM	2.1543	0.24	6.4537	1.48	8.9347	1.68	3.1889	0.88
10	LD4	2.1340	--	6.1531	--	9.1472	--	3.2157	--
	ED4	2.0843	2.33	5.8295	5.26	9.1330	0.15	3.2000	0.49
	16 HRM	2.1043	1.39	6.2094	0.91	9.2918	1.58	3.1952	0.64
	20 HRM	2.1287	0.25	6.0663	1.41	9.0102	1.50	3.1879	0.86
20	LD4	2.1155	--	6.0333	--	9.2966	--	3.2038	--
	ED4	2.0655	2.36	5.6891	5.71	9.2735	0.25	3.1866	0.54
	16 HRM	2.0854	1.42	6.0702	0.61	9.4396	1.54	3.1840	0.62
	20 HRM	2.1102	0.25	5.9400	1.55	9.1645	1.42	3.1763	0.86
50	LD4	2.1027	--	5.9564	--	9.3759	--	3.1929	--
	ED4	2.0525	2.39	5.5998	5.99	9.3473	0.30	3.1751	0.53
	16 HRM	2.0723	1.44	5.9816	0.42	9.5180	1.52	3.1736	0.57
	20 HRM	2.0973	0.26	5.8588	1.64	9.2470	1.38	3.1657	0.82
100	LD4	2.0981	--	5.9300	--	9.4006	--	3.1887	--
	ED4	2.0479	2.39	5.5692	6.08	9.3702	0.32	3.1706	0.57
	16 HRM	2.0677	1.45	5.9512	0.36	9.5423	1.51	3.1696	0.60
	20 HRM	2.0927	0.26	5.8309	1.67	9.2727	1.36	3.1615	0.85
1000	LD4	2.0938	--	5.9058	--	9.4220	--	3.1847	--
	ED4	2.0436	2.40	5.5413	6.16	9.3900	0.34	3.1664	0.58
	16 HRM	2.0634	1.45	5.9236	0.32	9.5635	1.50	3.1657	0.60
	20 HRM	2.0885	0.25	5.8054	1.68	9.2952	1.35	3.1576	0.85

6. Conclusions

This article presents the elastic bending problem solution of cross-ply doubly curved shells with constant curvature. Simply supported shells subjected to different types of mechanical loadings (bi-sinusoidal, uniform distributed, patch, hydrostatic and point load) are investigated. A two-dimensional hybrid refined models (HRMs) for shells, recently available in the literature is further studied in this manuscript. The HRMs are based in different combinations of trigonometric, exponential, zig-zag and Maclaurin polynomials thickness expansions. The governing equations are obtained using the Principle of Virtual Displacement and solved via Navier-closed form solutions. Transverse displacement w, normal stress $\sigma_{\alpha\alpha}$, transverse in-plane stress $\tau_{\alpha\beta}$, transverse shear stresses $\tau_{\alpha z}$, $\tau_{\beta z}$ and transverse normal stress σ_{zz} for different thickness ratios and curvature-radius-to-size are calculated. In general, this work investigates the capabilities of the HRMs for plates extended to shells subjected to different types of loading.

The following conclusions are described:

(1) Trigonometric functions showed better results over exponential functions for 0°/90°/0° lamination.
(2) The used of exponential, trigonometric and zig-zag shear functions in the kinematic models are mandatory for the adequate simulation of complex laminations as the one proposed by Demasi.
(3) It is concluded that for point loads, the static behavior of shells is better described with polynomial shear strain shape functions than with non-polynomial functions, due to the high gradients of the displacement fields on shell's top.
(4) The best model in predicting the transverse normal stress σ_{zz} for uniform distributed, patch and hydrostatic load is ED4.
(5) The best HRM model strictly depends on the type of loading, the stress or displacement to be analyzed and the curvature-to-side ratio. So it is verified that the best HRM in predicting the stresses and displacements is a *case dependent problem*.

Conflict of Interest

The author(s) declared no potential conflicts of interest with respect to the research, authorship and publication of this article.

Funding

This paper was written in the context of the project: "Diseño y optimización de dispositivos de drenaje para pacientes con glaucoma mediante el uso de modelos computacionales de ojos" founded by Cienciactiva, CONCYTEC, under the contract number N° 008-2016-FONDECYT. The authors of this manuscript appreciate the financial support from the Peruvian Government.

www.SID.ir

Archive of SID

References

[1] Jones, R.M., *Mechanics of composite materials*. Taylor and Francis, 1999.

[2] Hull, D., Clyne, T.W., *An introduction to composite materials*. Cambridge Solid State Science Series, 1996.

[3] Timoshenko, S., Woinowsky-Krieger, S., *Theory of plates and shells*. McGraw-Hill, 1959.

[4] Flügge, W., *Stresses in shells*. Springer-Verlag, 1960.

[5] Leissa, A.W., *Vibrations of shells*. NASA Sp. 288, 1973.

[6] Gould P.L., *Analysis of Shells and Plates*, Springer-Verlag, 1988.

[7] Soedel, W., *Vibrations of shells and plates*. Marcell Dekker, 2004.

[8] Love, A.E.H., The small free vibrations and deformation of a thin elastic shell. *Philosophical Transactions of the Royal Society A*, 179, 1888, 491-546.

[9] Hildebrand, F.B., Reissner, E., Thomas, G.B., Notes on the foundations of theory of small displacements of orthotropic shells. *NACA Technical Notes No. 1883*, 1949.

[10] Huang, N.N., Influence of shear correction factors in the higher order shear deformation laminated shell theory. *International Journal of Solids and Structures*, 31, 1994, 1263-1277.

[11] Shu, X.-P., A refined theory of laminated shells with higher-order transverse shear deformation. *International Journal of Solids and Structures*, 34, 1997, 673-683.

[12] Reddy, J.N., Liu, C.F., A higher-order shear deformation theory of laminated elastic shells. *International Journal of Engineering Science*, 23, 1985, 319-330

[13] Mantari, J.L., Oktem, A.S., Guedes Soares, C., Static and dynamics analysis of laminate composites and sandwich plates and shells by using a new higher order-shear deformation theory. *Composite Structures*, 94, 2011, 37-49.

[14] Mantari, J.L., Guedes Soares, C., Analysis of isotropic and multilayered plates and shells by using a generalized higher order shear deformation theory. *Composite Structures*, 94, 2012, 2640-2656.

[15] Thai, H.T., Ngugen, T.K., Vo, T.P., Ngo, T., A new simple shear deformation theory. *Composite Structures*, 171, 2017, 277-285.

[16] Demasi, L., Mixed plate theories based on generalized unified formulation, Part I: Governing equations. *Composite Structures*, 87, 2009, 1-11.

[17] Demasi, L., Mixed plate theories based on the generalized unified formulation. Part III: Advanced mixed high order shear deformation theories. *Composite Structures*, 87, 2009, 183-194.

[18] Demasi, L., Mixed plate theories based on the generalized unified formulation. Part V: Results. *Composite Structures*, 88 , 2009, 1-16.

[19] Caliri Jr., M.F., Ferreira, A.J.M., Tita, V., Through-the-thickness stress profiles in laminated composite and sandwich structure plates via unified formulation. *Composite Part B*, 107, 2016, 29-42.

[20] Oktem, S.A., Chaudhuri, R.A., Higher-order theory based boundary-discontinuous Fourier analysis of simply supported thick cross-ply doubly curved panels. *Computer & Structures*, 89, 2009, 448-458.

[21] Caliri Jr., M.F., Ferreira, A.J.M., Tita, V., A review on plate and shell theories for laminated and sandwich structures highlighting the finite element method. *Composite Structures*, 156, 2006, 63-77.

[22] Shimpi, R.P., Refined plates theory and its variants. *AIAA Journal*, 40, 2002, 137-145.

[23] Chen, H., Wang, A., Hao, Y., Zhang, W., Free vibration of FGM sandwich doubly curved shallow shell based on a new shear deformation theory with stretching effects. *Composite Structures*, 179, 2017, 50-60.

[24] Thai, H.T., Park, M., Choi, D.H., A simple refined theory for bending, buckling and vibration of thick plates resting on elastic foundation. *International Journal of Mechanical Sciences*, 73, 2013, 40-52.

[25] Ferreira, A.J.M., Roque, C.M.C., Jorge, R.M.N., Analysis of composites plates by trigonometric shear deformation theory and multiquadrics. *Composite Structures*, 83, 2005, 2225-2237.

[26] Mantari, J.L., Refined and generalized hybrid type quasi-3D shear deformation theory for the bending analysis of functionally graded shells. *Composites Part B: Engineering*, 83, 2015, 142-152.

[27] Filippi, M., Petrolo, M., Valvano, S., Carrera, E., Analysis of laminated composites and sandwich structures by trigonometric, exponential and miscellaneous polynomials and a MITC9 plate element. *Composite Structures*, 150, 2016, 103-114.

[28] Candiotti, S., Mantari, J.L., Yarasca, J., Petrolo, M., Carrera, E., An axiomatic/asymptotic evaluation for the best theories for isotropic and functionally graded plates employing non-polynomic functions. *Aerospace Science and Technology*, 68, 2017, 179-192.

[29] Yarasca, J., Mantari, J.L., Petrolo, M., Carrera, E., Best theory for cross-ply composite plates using polynomial, trigonometric and exponential thickness expansions. *Composite Structures*, 161, 2017, 362-383.

[30] Yarasca, J., Mantari, J.L., Petrolo, M., Carrera, E., Multiobjective best theory diagrams for cross-ply composites plates employing polynomial, zig-zag, trigonometric and exponential thickness expansions. *Composite Structures*, 176, 2017, 860-876.

[31] Yarasca, J., Mantari, J.L., N-objective genetic algorithm to obtain accurate equivalent single layer models with layer models with layerwise capabilities for challenging sandwich plates. *Aerospace Science and Technology*, 70, 2017, 170-188.

[32] Carrera, E., Cinefra, M., Lamberti, A., Petrolo, M., Results on best metallic and laminated shells including Layer-Wise

www.SID.ir

Archive of SID
models. *Composite Structures*, 126, 2015, 285-298.
[33] Mantari, J.L., Ramos, I.A., Zenkour, A.M., A unified formulation for laminate composite plates subjected to thermal loads using various plate theories. *International Journal of Applied Mechanics*, 8(8), 2016, 1650087.
[34] Panduro, R.M.R., Mantari, J.L., Hygro-thermo-mechanical behavior of classical composites using a new trigonometrical shear strain shape function and a compact layerwise approach. *Composite Structures*, 160, 2017, 378-391.
[35] Carrera, E., Valvano, S., Analysis of laminated composite structures with embedded piezo electric sheets by variable kinematic shell elements. *Journal of Intelligent Material Systems and Structures*, 28(20), 2017, 2959-2987.
[36] Brischetto, S., Carrera, E., Static analysis of multilayered smart shells subjected to mechanical, thermal and electrical loads. *Meccanica*, 48, 2013, 1263-1287.
[37] Giunta, G., Biscani, F., Belouettar, S., Carrera, E., Hierarchical modelling of doubly-curved laminated composites shells under distributed and localized loadings. *Composites Part B: Engineering*, 42, 2011, 682-691.
[38] Tornabene, F., Fantuzzi, N., Viola, E., Carrera, E., Static analysis of doubly-curved anisotropic shells and panels using CUF approach, differential geometry and differential quadrature method. *Composite Structure*, 107, 2014, 675-697.
[39] Dozio, L., A hierarchical formulation of the state-space Levy's method for vibration analysis of thin and thick multilayered shells. *Composite Part B: Engineering*, 98, 2016, 97-107.
[40] Viola, E., Tornabene, F., Fantuzzi, N., General higher-order shear deformation theories for free vibration analysis of completely doubly-curved laminated shells and panels. *Composites Structures*, 95, 2013, 639-666.
[41] Viola, E., Tornabene, F., Fantuzzi, N., Static analysis of completely doubly curved laminated shells and panels using general higher-order shear deformation theories. *Composites Structures*, 101, 2013, 59-93.
[42] Tornabene, F., Fantuzzi, N., Viola, E., Ferreira, A.J.M., Radial basis function method applied to doubly-curved laminated composite shells and panels with a general higher-order equivalent single layer formulation. *Composites Part B*, 55, 2013, 642-659.
[43] Thinh, T.I., Nguyen, M.C., Dynamic stiffness matrix of continuous element for vibration of thick cross-ply laminated composite cylindrical shells. *Composite Structures*, 98, 2013, 93-102.
[44] Cinefra, M., Valvano, S., A variable kinematic doubly-curved MITC9 shell element for the analysis of laminated composites. *Mechanical of Advance Materials and Structures*, 23, 2016, 1312-1325.
[45] Reddy, J.N., *Mechanics of laminated composite plates and shells, theory and analysis*. CRC Press, 1997.
[46] Carrera, E., Giunta, G., Hierarchical models for failure analysis of plates bent by distributed and localized transverse loadings. *Journal of Zhejiang University Science A*, 9(5), 2008, 600-613.
[47] Carrera, E., Multilayered shell theories accounting for layerwise mixed description part 1: Governing equations. *AIAA Journal*, 37, 1999, 1107-1116.
[48] Carrera, E., Multilayered shell theories accounting for layerwise mixed description part 2: Numerical evaluations. *AIAA Journal*, 37, 1999, 1117-1124.
[49] Cinefra, M., *Refined and advanced shell models for the analysis of advances structures*, PhD Thesis, Paris: University Paris Ouest – Nanterre La Defense, Torino: Politecnico di Torino, 2011.
[50] Thakur, S.N., Ray, C., Chakraborty, S., A new efficient higher-order shear deformation theory for a doubly curved laminated composite shell. *Acta Mechanica*, 228, 2017, 69-87.
[51] Tornabene, F., Fantuzzi, N., Bacciocchi, M., On the mechanics of laminated doubly-curved shells subjected to point and line loads. *International Journal of Engineering Science*, 109, 2016, 115-164.
[52] Ferreira, A.J.M., Carrera, E., Cinefra, M., Roque, C.M.C., Polit, O., Analysis of laminated shells by a sinusoidal shear deformation theory and radial basis functions collocation, accounting for through-the thickness deformations. *Composites: Part B*, 42, 2011, 1276-1284.
[53] Touratier, M., A refined theory of laminated shallow shells. *International Journal of Solid and Structures*, 29(11), 1992, 1401-1415.
[54] Mantari, J.L., Oktem, A.S., Guedes Soares, C., Bending and free vibration analysis of isotropic and multilayered plates and shells by using a new accurate higher-order shear deformation theory. *Composites: Part B*, 43, 2012, 3348-3360.
[55] Murakami, H., Laminated composite plate theory with improved in-plane responses. *Journal of Applied Mechanics*, 53(3), 1986, 661-666.
[56] Canales, F.G., Mantari, J.L., A boundary-discontinuous based Fourier analysis of thick laminated beam via 1D-CUF model. *International Journal of Solids and Structures*, 118-119, 2017, 109-118.
[57] Canales, F.G., Mantari, J.L., Discrepancy on the free vibration of laminated composite plates coupled to a compressible and incompressible fluid domain. *Ocean Engineering*, 167, 2008, 267-281.
[58] Canales, F.G., Mantari, J.L., An assessment of fluid compressibility influence on the natural frequencies of a submerged plates via unified formulation. *Ocean Engineering*, 147, 2018, 414-430.
[59] Carrera, E., Giunta, G., Petrolo, M., *Beam Structures Classic and Advanced theories*. John Wileys & Sons, 2011.
[60] Monge, J.C., Mantari, J.L., Charca, S., Vladimir, N., An axiomatic/asymptotic of the best theories for the free vibration of laminated and sandwich shells using non-polynomial functions. *Engineering Structures*, 172, 2018, 1011-1024.
[61] Carrera, E., Petrolo, M., Guidelines and recommendations to construct theories for metallic and composite plates. *AIAA Journal*, 48(12), 2010, 2852-2866.
[62] Brischetto, S., Tornabene, F., Advanced GDQ models and 3D stress recovery in multilayered plates, spherical and double-

www.SID.ir

curved panels subjected to transverse shear loads. *Composite Part B: Engineering*, 146, 2018, 244-269.
[63] Tornabene, F., Salvatore, B., 3D capability of refined GDQ models for the bending analysis of composite and sandwich plates, spherical and doubly-curved shells. *Thin Walled Structures*, 129, 2018, 94-124.

Appendix A

The implicit version of the fundamental nuclei are listed below. The next in plane coefficients must be considered: $\bar{\alpha}=m\pi/a, \bar{\beta}=n\pi/b$ with m and n as the wave numbers and a and b as the size of the shell panel. The following integration over the thickness must be considered:

$$\begin{aligned}
&\left(J^{k\tau s},J^{k\tau s}_{\frac{\alpha}{\beta}},J^{k\tau s}_{\frac{\beta}{\alpha}}\right)=\int_{A_k}\left(F_\tau F_s,F_\tau F_s\frac{H^k_\alpha}{H^k_\beta},F_\tau F_s\frac{H^k_\beta}{H^k_\alpha}\right)dz\\
&\left(J^{k\tau_z s}_{\alpha},J^{k\tau_z s}_{\beta}\right)=\int_{A_k}\left(F_{\tau_z}F_s H^k_\alpha,F_{\tau_z}F_s H^k_\beta\right)dz\\
&\left(J^{k\tau s_z}_{\alpha},J^{k\tau s_z}_{\beta}\right)=\int_{A_k}\left(F_\tau F_{s_z} H^k_\alpha,F_\tau F_{s_z} H^k_\beta\right)dz\\
&J^{k\tau_z s_z}_{\alpha\beta}=\int_{A_k}F_{\tau_z}F_{s_z}H^k_\alpha H^k_\beta dz
\end{aligned}\tag{A.1}$$

The fundamental nuclei $K^{k\tau s}_{uu}$ are expressed as follows:

$$\begin{aligned}
K^{k\tau s}_{uu11}&=\bar{\alpha}^2C^k_{11}J^{k\tau s}_{\frac{\beta}{\alpha}}+C^k_{55}\left(J^{k\tau_z s_z}_{\alpha\beta}-\frac{J^{k\tau s_z}_{\beta}}{R^k_\alpha}-\frac{J^{k\tau_z s}_{\beta}}{R^k_\alpha}+\frac{1}{R^{k\,2}_\alpha}J^{k\tau s}_{\frac{\beta}{\alpha}}\right)+\bar{\beta}^2C^k_{66}J^{k\tau s}_{\frac{\alpha}{\beta}}\\
K^{k\tau s}_{uu12}&=\bar{\alpha}\bar{\beta}J^{k\tau s}\left(C^k_{12}+C^k_{66}\right)\\
K^{k\tau s}_{uu13}&=C^k_{55}\left(\bar{\alpha}J^{k\tau_z s}_{\beta}-\bar{\alpha}\frac{1}{R^k_\alpha}J^{k\tau s}_{\frac{\beta}{\alpha}}\right)-\bar{\alpha}C^k_{13}J^{k\tau s_z}_{\beta}-\frac{\bar{\alpha}C^k_{11}}{R^k_\alpha}J^{k\tau s}_{\frac{\beta}{\alpha}}-\frac{\bar{\alpha}C^k_{12}}{R^k_\beta}J^{k\tau s}\\
K^{k\tau s}_{uu21}&=\bar{\alpha}\bar{\beta}J^{k\tau s}\left(C^k_{12}+C^k_{66}\right)\\
K^{k\tau s}_{uu22}&=\bar{\alpha}^2C^k_{66}J^{k\tau s}_{\frac{\beta}{\alpha}}+C^k_{44}\left(J^{k\tau_z s_z}_{\alpha\beta}-\frac{J^{k\tau s_z}_{\alpha}}{R^k_\beta}-\frac{J^{k\tau_z s}_{\alpha}}{R^k_\beta}+\frac{1}{R^{k\,2}_\beta}J^{k\tau s}_{\frac{\alpha}{\beta}}\right)+\bar{\beta}^2C^k_{22}J^{k\tau s}_{\frac{\alpha}{\beta}}\\
K^{k\tau s}_{uu23}&=C^k_{44}\left(\bar{\beta}J^{k\tau_z s}_{\alpha}-\bar{\beta}\frac{1}{R^k_\beta}J^{k\tau s}_{\frac{\alpha}{\beta}}\right)-\bar{\beta}C^k_{23}J^{k\tau s_z}_{\alpha}-\frac{\bar{\beta}C^k_{22}}{R^k_\beta}J^{k\tau s}_{\frac{\alpha}{\beta}}-\frac{\bar{\beta}C^k_{12}}{R^k_\alpha}J^{k\tau s}\\
K^{k\tau s}_{uu31}&=C^k_{55}\left(\bar{\alpha}J^{k\tau s_z}_{\beta}-\bar{\alpha}\frac{1}{R^k_\beta}J^{k\tau s}_{\frac{\beta}{\alpha}}\right)-\bar{\alpha}C^k_{13}J^{k\tau_z s}_{\beta}-\frac{\bar{\alpha}C^k_{11}}{R^k_\alpha}J^{k\tau s}_{\frac{\beta}{\alpha}}-\frac{\bar{\alpha}C^k_{12}}{R^k_\beta}J^{k\tau s}\\
K^{k\tau s}_{uu32}&=C^k_{44}\left(\bar{\beta}J^{k\tau s_z}_{\alpha}-\bar{\beta}\frac{1}{R^k_\beta}J^{k\tau s}_{\frac{\alpha}{\beta}}\right)-\bar{\beta}C^k_{23}J^{k\tau_z s}_{\alpha}-\frac{\bar{\beta}C^k_{22}}{R^k_\beta}J^{k\tau s}_{\frac{\alpha}{\beta}}-\frac{\bar{\beta}C^k_{12}}{R^k_\alpha}J^{k\tau s}\\
K^{k\tau s}_{uu33}&=\bar{\alpha}^2C^k_{55}J^{k\tau s}_{\frac{\beta}{\alpha}}+\bar{\beta}^2C^k_{44}J^{k\tau s}_{\frac{\alpha}{\beta}}+C^k_{33}J^{k\tau_z s_z}_{\alpha\beta}+\frac{1}{R^k_\alpha}\left(\frac{C^k_{11}}{R^k_\alpha}J^{k\tau s}_{\frac{\beta}{\alpha}}+C^k_{13}J^{k\tau s_z}_{\beta}+C^k_{13}J^{k\tau_z s}_{\beta}\right)+\\
&\frac{1}{R^k_\beta}\left(\frac{C^k_{22}}{R^k_\beta}J^{k\tau s}_{\frac{\alpha}{\beta}}+C^k_{23}J^{k\tau s_z}_{\alpha}+C^k_{23}J^{k\tau_z s}_{\alpha}\right)+\frac{2C^k_{12}}{R^k_\alpha R^k_\beta}J^{k\tau s}
\end{aligned}\tag{A.2}$$

© 2019 by the authors. Licensee SCU, Ahvaz, Iran. This article is an open access article distributed under the terms and conditions of the Creative Commons Attribution-NonCommercial 4.0 International (CC BY-NC 4.0 license) (http://creativecommons.org/licenses/by-nc/4.0/).